THE EFFECT OF NIOBIUM ON THE HEAT-AFFECTED-ZONE TOUGHNESS OF ARCTIC GRADE LINE PIPE

(UP-S-457)

INTERIM REPORT BY STELCO INC.

Work on this project was conducted under the auspices of the Canada Centre for Mineral and Energy Technology, Energy, Mines and Resources, Canada

DSS File Number:	26SQ.23440-3-9025
DSS Contract Serial Number:	ISQ83-00020
CANMET Project Number:	420603
CANMET Scientific Authority:	M. Godden

60 pp

February 1985
R&D Report No. 85R030

OCT 30 1985

MICROMEDIA

RÉSUMÉ

L'effect des addition de Nb sur la résistance et la ténacité du metal de base et sur la structure de la ZAT simulé a été determiné pour la pipe line d'acier nuance 483. Nb a 0,015 et 0,044 pourcent ajouté a la composition de base a augmenté significativement la résistance du metal de base, aussi que celle de la ZAT. Tandis que les additions de Nb a produit un affinement du grain dans le metal de base laminé sous contrôle ils n'y avaient presque aucun effect sur la température de transition Charpy a cause de effets contraire d'affinement du grain et durcissement par precipitation sur la comportment de la transition rupturelle. Les additions de Nb n'a peu modifié la structure métallographique de la ZAT développé en éprouvettes de simulation avec un apport d'énergie de 2 kJ/mm. Mesures dilatométriques de la comportment de la transformation a confirmé q'un contenu élevé du Nb a peu diminué les températures de transformations. La ténacité de la ZAT, mesuré également pars essais CTOD et Charpy, a détérioré signifigativement avec un accroissement de la teneur en Nb. Le changement en température de transition Charpy et CTOD peut être rapporté quantitativement avec l'accroissement en résistance de la ZAT.

EXECUTIVE OVERVIEW

The effect of Nb additions on the strength and toughness of the base plate and simulated HAZ structure of a C-Mn-Mo-Ti grade 483 line pipe steel has been determined. Additions of 0.015 and 0.044 percent Nb to a base chemistry significantly increased both base plate and HAZ strength. Although the Nb additions developed a finer ferrite grain size in the controlled rolled base plate, little or no change in base plate Charpy transition temperature was found because of the offsetting effects of grain refinement and precipitation strengthening on fracture transition behavior. Nb additions did not significantly alter the HAZ microstructure, developed with the 2 kJ/mm heat input simulation. Dilatometer measurements of the transformation behavior confirmed that increased Nb content only slightly lowered the transformation temperatures. The HAZ toughness, measured by both CTOD and Charpy tests, deteriorated significantly with increased Nb content. The shift in Charpy and CTOD transition temperature can be quantitatively related to the increase in HAZ strength.

Project Title: Effect of Niobium on Heat-Affected-Zone Toughness of Arctic Grade Line Pipe (UP-S-457)

DSS Number: ISQ83-00020

Date: February 23, 1985

Company:
Stelco Inc.
Royal Trust Tower
Toronto Dominion Centre
Toronto, Ontario

Proposal Submitted By:
Mr. J. C. McKay
Director, Research and Development
Stelco Inc.
Hamilton, Ontario
L8N 3T1

CONTENTS

Introduction..... 6

Procedure..... 8

Results..... 11

Discussion..... 17

Prediction of Charpy Transition Temperature..... 22

Prediction of CTOD Transition Temperature..... 23

Prediction of Transition Temperature in CTOD Tests..... 25

Conclusions..... 26

Further Work..... 26

Acknowledgments..... 28

References..... 29

INTRODUCTION

The material property specifications for large diameter gas transmission line pipe have included fracture resistance criteria both to minimize the risk of fracture initiation and to ensure crack arrest in the event of failure. Over the last two decades line pipe development has primarily focused on determining those factors which control fracture arrest and on developing steelmaking and controlled rolling practices to produce high toughness in the pipe body. More recently, some line pipe specifications have introduced toughness requirements for the pipe seam weld zone. Welding consumables and processes have been developed to ensure adequate fracture resistance in the weld metal; however, there has been little research to improve the toughness of the weld heat-affected-zone (HAZ).

Most of the studies of the mechanical properties of HAZs have been related to welded joints in structural steels, ship plate and pressure vessel steels. It has been shown that the toughness of the coarse-grained HAZ next to the weld fusion line is almost always lower than that of the base metal.[1-3] Also, it has been demonstrated that the HAZ toughness deteriorates with increased heat input,[4] and is lowered by vanadium and niobium additions, particularly in high input welds (>2 KJ/mm).[5-7]

There have been a limited number of investigations on the HAZ properties of line pipe weld seams. These tests have generally shown that the HAZ fracture initiation resistance of conventional line pipe steels (Grades

414 to 483) is low.[8-9] Offshore line pipe producers have addressed this problem and are now developing alternate steel chemistries[10-11] and welding procedures[12-13] to improve HAZ toughness; however, there has been very little work within the North American line pipe industry to either characterize or improve HAZ fracture initiation resistance.

Previous research conducted jointly by CANMET and Stelco has demonstrated that the HAZ toughness of Grade 483, C-Mn-Mo-Nb type, line pipe can be markedly improved by the addition of 0.01 percent titanium.[14] The improvement in toughness was related to control of grain coarsening in the HAZ by stable TiN precipitates originating in the cast structure. More recent work[15] has suggested that increased Nb content has a detrimental effect on the HAZ ductile to brittle transition temperature. However, the mechanism for this decrease in fracture resistance was not clearly established. The objectives of the present study were:

- to characterize the ductile and cleavage fracture resistance of the base plate and HAZ structures for a Grade 483 pipe steel with a range of niobium contents,
- to relate the fracture parameters to the detailed microstructure, and
- to determine the effect of Nb on HAZ hardenability and microstructure.

Procedure

Laboratory heats were made to a partially acicular ferrite, C-Mn-Mo base chemistry, containing 0.01 percent Ti (Table I). Three levels of Nb were studied 0, 0.015 and and 0.044 percent. Each heat was induction melted and cast into iron-chilled sand molds (200 x 130 x 150 mm) designed to achieve an average cooling rate similar to that of a continuously cast slab.

A 130 x 150 x 180 mm (t x w x l) slab was cut from each ingot. Each slab was reheated and hot rolled to 15 mm plate using the following controlled rolling practice:

- maximum reheat temperature 1220°C
- roughing (10 passes) to 63 mm between 1095 and 925°C
- finishing (9 passes) to 15 mm between 895 and 775°C

Full size, transverse (Figure 1) Charpy V-notch transition curves were broken from each base plate. Both longitudinal and transverse tensile tests were performed over a range of temperatures between +20 and -50°C, using at least two samples at each temperature.

The as-rolled microstructures were quantified in terms of grain size and volume fraction of ferrite using a QTM 720 image analyzer. The cleavage facet size on the fracture surface of a low temperature (-196°C) Charpy test was measured using a linear intercept method on SEM micrographs.

Studies of the HAZ strength and toughness involved testing 10 x 10 x 65 mm samples thermally cycled in a Gleeble weld simulator to reproduce the effects of a single pass, 2 KJ/mm heat input submerged-arc weld. All samples were oriented transverse to the plate rolling direction. The simulated HAZ fracture resistance was measured by both Charpy V-notch and fatigue precracked crack tip opening displacement (CTOD) transition curves. The CTOD tests were done in accordance with British Standard 5762 (1979). A minimum of two and as many as four CTOD tests were done at each temperature over a range of temperatures between +52 and -32°C. After testing each sample was sectioned and metallographically prepared to measure the prior austenite grain size and microhardness, and to identify the transformation products in the simulated HAZ. Also, the cleavage facet size was measured on selected HAZ Charpy fracture surfaces using the SEM.

The HAZ strength was measured using 4 mm diameter round bar tensiles whose gauge length (8 mm) was machined from the Gleeble samples to correspond to the uniform HAZ structure. All tests were oriented transverse to the plate rolling direction. HAZ tensiles were tested over a range of temperatures between +20 and -50°C.

In addition to clip gauge measurement of the CTOD, a new method was developed to measure the ductile crack initiation resistance (δ_i)[16] of both base plate and Gleeble simulated HAZs. δ_i is essentially a material parameter which, unlike other measures (δ_m, δ_c) is independent of constraint effects (sample thickness). The definition of δ_i required for macroscopic crack initiation toughness is not exact.

This is partly due to the inability of existing methods to accurately measure δ_i over the entire crack front.

Some previous work has considered data points associated with crack extensions of less than 0.15 mm to be invalid,[17] and have extrapolated macrocrack data through the microcrack regime. Others have used δ_m[18], the CTOD of maximum load. In the current work, direct observation of the microstructural damage during progressive loading enabled microcrack development to be studied for crack extensions less than 0.15 mm.

The method of observation was as follows. Notched bar samples (10 x 10 x 65 mm) were fatigue precracked to give an a/w of 0.50. Base plate tests were taken in both the TS and TL orientations, whereas the HAZ tests were done only in the TL orientation (Figure 1). After precracking, the samples were loaded in three point bending in the device shown in Figure 2, and the loaded samples placed in an SEM for examination of the notch root. The samples were incrementally loaded, and after each increase in load the entire crack front of the specimen was scanned at 320 magnification, and the total lengths of the microcracks and microvoids measured. A series of typical micrographs showing development of microvoid along the fatigue crack notch root are shown in Figure 3. For the sample geometry used, the plane strain thickness (B_o) along the notch root is between 7 and 8 mm. When initiation had occurred along the entire crack front, the specimen was overloaded to extend the macroscopic crack. The crack extension was measured by either heat tinting the samples at 300°C for 40 minutes or breaking the samples after cooling in liquid nitrogen. The width of the

ductile crack extension zone was measured with an optical microscope to determine the Δa for the crack.

To assess the potential change in HAZ transformation characteristics with Nb additions, dilatometric measurements of each steel were made at the PMRL labs of CANMET. The dilatometer specimens were reheated to 1350°C (within six seconds) and cooled using a series of cycles to give $\Delta T_{800-500°C}$ of between ≈3.5 and 245 seconds.

Results

1. Metallography

In the as-rolled condition, all steels developed a partially acicular ferrite type microstructure consisting of polygonal ferrite and bands of degenerate pearlite and upper bainite with islands of martensite-retained austenite (M/A) constituent. SEM micrographs of the as-rolled structures are shown in Figure 4a. The Nb microalloyed steels had a slightly finer ferrite grain size than the non-Nb steel (4.5 versus 6.0 microns). This difference is attributed to the effect of Nb on retarding austenite recrystallization during finishing. Limited TEM microscopy of the Nb free and highest Nb steel revealed ≈300 Å precipitates in the Nb bearing steel (Figure 4b). No diffraction measurements were made on these particles and thus it is not possible to comment on their origin based upon the compositional work done previously[14] on a similar chemistry.

The Gleeble simulated HAZs showed a lamellar bainitic structure, consisting of both ferrite and sub-micron particles of M/A constituent (Figure 5). The prior austenite grains sizes for all steels showed a relatively wide distribution, ranging from less than 30 to over 100 microns within a sample (Figure 6). The mean grain sizes for all three steels were similar - 55 μm for the non-Nb steel and approximately 70 μm for the two Nb bearing steels.

2. Tensile Properties

In the as-rolled condition, the yield stress level increased significantly (from ≈320 to over 440 MPa) with increasing Nb content (Figure 7). This increase in yield strength is believed to result mainly from precipitation strengthening of ferrite by Nb (C, N) particles. An estimate of the strengthening contribution based on the work of Brown et al[19] assuming the observed (≈320 Å) precipitate size accounts for only 40 MPa of the actual (120 MPa) strength increase. Much finer precipitates, not resolved in the TEM study, are believed to account for the balance of the strength increase.

All steels showed continuous stress strain behavior over the entire range of test temperatures. The "round-house" stress strain curve results from the residual stresses and free dislocations occurring due to the M/A constituent in the microstructure.

The yield stress increased only slightly with decrease in test temperature (Figure 7), however, the UTS showed a much more marked increase with temperature reduction. It should be noted that in considering the temperature dependence of strength, that the UTS depends on both the yield stress and the strain hardening rate, and hence the temperature dependence on the yield stress and UTS need not be identical.

The HAZ (Gleeble) samples had significantly higher yield and ultimate tensile strength than the as-rolled plate. Increasing the Nb content resulted in significantly higher HAZ strengths over the temperature range tested (Figure 8). The higher strength of the HAZs reflects the change from a largely polygonal ferrite structure to an upper bainitic structure. As with the base plate, the HAZ stress strain curves were continuous in form, which is a result of the significant M/A phase present and residual stresses resulting from the bainite transformation. Also, the yield strengths were relatively independent of temperature, whereas the ultimate tensile strengths increased with decreasing temperature.

3. Dilatometry

The metallography of the HAZ samples showed little difference in the transformed microstructures of the three steels. The dilatometer tests defined a slight lowering in the transformation temperatures with increased Nb additions (Table II). This reduction, while significant, would not be expected to noticeably alter the HAZ microstructure since

all of the structures were transformed at temperatures within the "upper bainite" regime.

4. Fracture Properties

The Nb additions did not result in a major shift in the as-rolled plate Charpy transition curves (Figure 9). Although the Nb-bearing steels had slightly finer ferrite grain sizes than the non-Nb steel, the effect of this on reducing the transition temperature was offset by the increased precipitation strengthening due to Nb additions. The HAZ Charpy transitions were more sensitive to Nb additions (Figure 10) than those for the as-rolled plate. The non-Nb steel showed the lowest impact transition temperature.

In order to rationalize the changes in fracture resistance with Nb content it was necessary to consider the microstructural features controlling the cleavage fracture in the base plate and HAZ. Detailed fractographic studies on the base plate revealed that the cleavage facets were well defined and essentially flat (Figure 11a) whereas the HAZ fracture surfaces were rough and exhibited extensive river markings (Figure 11b). Using the two-surface technique[20] to observe the fracture surface and etched microstructure revealed that the irregular structures corresponded to the passage of the crack front through lamellar ferrite laths (Figure 12).

The cleavage facet sizes for the HAZ were significantly larger than those for the base plate (Figure 13). Whereas the base plate facet sizes were all of the order of 8 μm, the HAZ facets were about 30 μm. It is notable that the facet size distributions, like the ferrite grain and prior austenite grain size distributions showed significant variance about the mean. Also, the fact that the average facet size in the base plate is greater than the average grain size indicates that the fracture resistance appears to be controlled by the larger ferrite grains, possibly because they are contiguous in the microstructure, and thus the cleavage fracture stress is controlled by the largest grains rather than the average grain size.

The HAZ cleavage facets (Figure 14) were markedly smaller than the prior austenite grain size, suggesting that a sub-unit of the prior austenite grain - presumably the bainite colony size - controls the cleavage process. The slight corrugation of the cleavage facets, related to the intersection of ferrite lath boundaries is thought to have little effect on the cleavage stress.

It is of interest that the as-rolled plate Charpy fracture surfaces exhibited significant splitting over the temperature range between -25 and -110°C (Figure 15), whereas the HAZ samples showed virtually no splitting (Figure 16). In the one HAZ test with a major split, the delamination was inclusion related. The splitting in the base plate is believed to be associated with ferrite texture (caused by controlled rolling below the Ar_3 temperature) and the inherent weaknesses of the ferrite-non-ferrite band interfaces. The effect of splitting on the

base plate percent shear transition is to lower it by promoting plane stress ductile fracture. However, the cleavage initiation temperature (≈20 J temperature) is not altered by splitting because it does not occur at this low energy level.

The CTOD HAZ tests also showed a reduction in fracture initiation resistance with Nb additions. Table III summarizes the minimum CTOD values at each temperature for each steel. The Nb-free steel again showed the lowest 0.1 mm CTOD crack initiation temperature. Increasing the Nb content from 0 to 0.015 to 0.044 percent significantly increased the cleavage crack initiation temperature.

The room temperature micro- and macro-crack resistance curves of the base plate and simulated HAZ samples are shown in Figures 17, 18 and 19. The parameter c/Bo describes the linear fraction of the notch root length occupied by voids. It does not take any cognizance of void distribution along the notch root. The base plate tests were done in both the TL and TS direction. It is notable that all three steels showed much higher crack initiation resistance (δ_i) in the TS direction than in the TL direction. This presumably occurs because of the potential for delamination or lateral relaxation that occurs at the crack tip when the crack front is moving in the through-thickness direction. Although there was little difference in the crack initiation resistance between the three steels when tested in the TS direction, the Nb free steel had a higher δ_i value than the two Nb-bearing steels when tested in the TL direction. This may result from the lower strength (i.e. lower flow stress) of the Nb-free steel which would tend

to increase the critical strains needed for micro-void initiation and coalescence.

The simulated HAZs of all three steels exhibited similar room temperature micro-crack resistance curves (Figure 19) except that the highest Nb level exhibited cleavage "pop-in" at δ = 0.15 mm and C/Bo ≈0.8. The δ_i (temperature independent) ductile crack initiation resistance values for each steel is estimated to be ≈0.19 mm.

These measurements of crack initiation resistance are in good agreement with those obtained by clip gauge measurement. In the tests done with clip gauge, the highest Nb steel had a room temperature, δ_c, value of 0.11 mm compared with 0.17 for the 0.15 Nb steel and 0.22 for the Nb-free steel.

The fact that the three HAZ structures exhibited micro-crack resistance curves similar to those of the base plate suggests that the micro-crack initiation and coalescence is not too dependent on microstructural features other than inclusion content. Figure 20 shows voids nucleated at inclusions in a simulated HAZ sample. Void initiation was not found to be related to the upper bainite microstructural features.

Discussion

In order to rationalize the observed shift in the simulated HAZ Charpy V-notch and CTOD transition behavior, it is necessary to quantify the effect of niobium on the cleavage fracture and yield stress, and to

relate these to the factors controlling ductile-brittle transition, based on the Orowan approach.[17] To facilitate this analysis, two methods of estimating the cleavage fracture stress were used:

- the Cottrell[18] relationship with grain size. This has uncertainties because of the influence of grain boundary carbides, and the non-ideal fracture unit of bainitic HAZ microstructure, and
- the Charpy 20 J transition temperature. If it is assumed that cleavage fracture occurs at general yield, it is possible to calculate the cleavage fracture stress using the stress intensification factor.

Originally, it was also considered that the low temperature fracture resistance could be assessed by measuring the effect of notch root radius on toughness in the manner developed by Malkin and Tetelman.[21] However, problems are encountered in using this approach. In structural steels, the cleavage process is nucleated heterogeneously at second phase particles or twin intersections. The process of cleavage initiation depends not only on the operating value of the maximum tensile stress but also on the location of the nucleating sites in the stress field of the initiating notch or crack. Moreover, the criteria for brittle fracture are dependent on the size and geometry of the sample. For this reason we have not attempted to directly measure the cleavage fracture stress but have used the approaches described below to estimate this quantity, in order to rationalize the effect of Nb addition.

It is important to stress that the objective of this section of the discussion is to provide a framework for rationalization of the influence of Nb additions on HAZ fracture behavior. In complex commercial materials it is difficult to make direct measurement of parameters such as the critical stress for fracture. Further, the amount of available data is limited, and thus our objective here has been to provide a basic model for rationalizing the data and some self-consistent tests for the model. Given these important limitations, however, it is reasonable to consider a variety of methods of estimating the fracture stress in terms of the microstructural parameters of the steel.

1. Cottrell Analysis

Previous work by Almond et al[22] has confirmed that the cleavage fracture stress can be related to the controlling "grain" size and the carbide thickness (Figure 21). SEM analysis of the HAZ and base plate fracture surfaces indicated that the central cleavage facet sizes were ≈30 μm and 8 μm, respectively. Assuming that similar criteria apply to both ferrite and bainitic steels, the cleavage fracture stresses are estimated to be ≈1500 MPa and 2500 MPa for the HAZ and base plate, respectively.

2. Charpy-Energy Transition Temperature

The cleavage fracture stress, σ^*_f, can be measured or calculated from

$$\sigma^*_f = Q\sigma_y \qquad ...(1)$$

where Q is the stress intensification factor.

At the point of general yield, Q is 2.57 in a four point bend test for specimens of Charpy geometry (a/w = 0.2).

Assuming Q = 2.57 for the Charpy test, and that the general yield load, P_{gy}, can be calculated by

$$P_{gy} = 1.5\ B/S\ (w-a)^2\ \sigma_{ys} \qquad ...(2)$$

where: B = test thickness (m)

S = test span (m)

w = test width (m)

a = notch depth (m)

σ_y = unaxial yield stress (MPa)

and that the displacement in a three-point bend test is

$$\Delta = P/BE\ 14.0\ (1-a/w)^{-2} \qquad ...(3)$$

where: P = load (N)

E = Young's modulus (MPa)

The elastic energy, A_{el}, absorbed at general yielding can be estimated by

$$A_{el} = 1/2\ P\Delta \qquad ...(4)$$

Assuming that the dynamic yield stress, σ_{yd}, in the Charpy test is predicted by

$$\sigma_{yd} = \sigma_{ys} + 175 \text{ MPa}^{23} \qquad \ldots(5)$$

and that σ_{ys} = 610 MPa and a = 2 mm, the elastic energy absorbed at general yield is estimated to be approximately 2 J.

Considering the increase in energy due to plastic straining, the fracture energy after achieving maximum load, and the energy absorbed in the testing system, it is reasonable to assume that the total energy absorption when cleavage fracture occurs at the general yield load is the order of 10-20 J. Using the 20 J criteria for cleavage fracture at general yield, it is possible to calculate the dynamic yield strength based on the tensile yield strength measured at the temperature corresponding to the 20 J temperature.

For the simulated HAZ structure, the estimated cleavage fracture stress ranges between ≈1800 and 2000 MPa for the non-Nb and 0.044 percent Nb steels, respectively. The difference results from the slight change in HAZ strength at the 20 J transition temperature. This estimate is in good agreement with that from the Cottrell approach.

For the base plate condition yield strength data was not obtained at the temperatures corresponding to the 20 J Charpy transition in the range -140°C to -160°C. However, assuming an average T_{20J} for all steels of -150°C, σ_{yd} can be estimated from the following formula.[21]

$$\sigma_{yd}\ (MPa) = \sigma_{ys} + \frac{1.20 \times 10^6}{\log\ (2 + t \times 10^{10})(1.8\ T + 491)} - 189 \qquad ...(6)$$

where: t = loading time ≈ 400 μs

T = -140°C

σ_{ys} = yield strength (MPa) at room temperature

For the range of base plate yield strength tested (320 to 450 MPa), the dynamic yield stress would be predicted to range between ≈890 to 1020 MPa at -140°C. The corresponding cleavage fracture stress is estimated to range between ≈2300 and 2600 MPa, which again is in good agreement with number predicted from the Cottrell approach, assuming a base plate cleavage facet size of 8 μm and a carbide thickness of the order of 0.1 to 0.2 μm.

Prediction of Charpy Transition Temperature

Using the estimation of cleavage fracture stress (2000 and 2600 MPa for the simulated HAZ and base plate, respectively) an estimate of the 20 J transition temperature can be made by the previously used formula, using the room temperature yield stress data (Table IV).

The actual transition data agree well with the predicted temperatures. Figure 22 shows schematically the shift in transition temperature resulting from the differences in cleavage fracture stress and yield stress for both base plate and HAZ. Figure 23 shows the predictions for each steel, and demonstrates the shift in transition resulting from the Nb additions. It is important to note that the effect in the dynamic yield strength due to Nb addition results in a much larger shift in cleavage initiation transition temperature for the HAZ structure than the base plate structure. The data shown in Figure 23 are intended to illustrate the changes which are due to simultaneous increases in the yield stress and decreases in the fracture stress. At present, however, there is insufficient data over the total range of temperature to conclude that the method used is predictive in other cases.

Prediction of CTOD Transition Temperature

Using the method described above for notched specimens, it is also possible to rationalize the variation of CTOD (fatigue precracked) transition temperature. The important concept developed here is that initial voiding may develop into either fully ductile initiation or cleavage depending on the yield and cleavage stress levels. This gives rise to an initiation mechanism transition temperature which can be determined. It is important to note, however, that this temperature is very dependent on the degree of constraint, i.e. sample size, and thus some form of characterization of constraint effects is required to extend this model to make it applicable to design.

In the case of fatigue precracked tests, various transition criteria can be defined. From the microcrack transition curve, these include (Figure 24):

δ_i - ductile macrocrack initiation

δ_{io} - ductile microcrack initiation

Δ_{ao} - corresponding crack extension at macrocrack initiation

δ_m - CTOD at max load P_M

Δ_{am} - ductile crack extension at maximum load P_M

δ_{clv} - cleavage crack initiation which may occur before or after ductile crack initiation

T_i - macrocrack initiation mechanism transition temperature where $\delta_{clv} = \delta_i$

Tio - microcrack initiation mechanism transition temperature where $\delta_{clv} = \delta_{io}$

Based on these definitions the crack initiation mechanisms can be classified as follows:

CTOD	Crack Initiation Mechanism
$\delta_{clv} < \delta_{io}$	pure cleavage
$\delta_{io} < \delta_{clv} < \delta_i$	mixed
$\delta_i < \delta_{clv}$	pure ductile

T_{clv} corresponds to the maximum temperature at which cleavage fracture can take place. Hence, when $T > T_{clv}$ cleavage fracture can never take place, and $\delta_{clv} \to \infty$.

For the base plate condition, all three steels exhibited ductile fracture in the Charpy-size sample at room temperature. Also T_i was lower than -50°C (i.e. ductile crack initiation). In contrast, the room temperature fracture mechanisms (i.e. initiation and instability) were entirely different for the HAZ samples of the three steels. As shown schematically, in Figure 25, the Nb free steel exhibited ductile initiation and instabilitly, whereas the higher Nb level showed cleavage mechanisms. The 0.015 Nb steel initiated in a ductile manner, but instability occurred by cleavage. The corresponding δ_i and δ_{clv} values and the crack initiation mechanism transition temperature, T_i are given in Table V.

Prediction of Transition Temperature in CTOD Tests

For the CTOD tests, the transition temperature T_i is the temperature at which cleavage instability occurs just at the moment of linkage of the microcrack at the entire crack front (i.e. $\delta_i = \delta_{clv}$). For the simulated HAZ tests, the three steels tested had almost the same prior austenite grain size and ductile crack initiation δ_i value. Thus, it is reasonable to expect that when $\delta = \delta_i$ for these steels, that their stress intensification factor, Q, would be similar. The value of Q can be estimated from the experimental data for the 0.015 Nb steel because at room temperature $\delta_{clv} \approx \delta_i$. For a yield stress value of 575 MPa, and cleavage stress of 2000 MPa, the corresponding Q value is 3.5. Asssuming that the yield stress of the HAZ under CTOD test conditions (loading time t = ≈100 sec) can be calculated by equation 6, the transition temperature was estimated. These values and the values determined from the actual CTOD tests are tabulated in Table VI.

There is fairly good agreement between these values. Slight differences in the calculated cleavage stress values for these steels or errors in the yield stress values calculated from equation would be expected to account for the observed differences between the actual and calculated T_i values.

Conclusions

Nb additions to a C-Mn-Mo type line pipe chemistries have been shown to increase the ductile-cleavage fracture initiation transition temperature of both the as-rolled steel and the submerged-arc weld HAZ. The apparent reduction in fracture resistance of the HAZ structure is significantly greater than that observed for the as-rolled plate. This effect can be rationalized in terms of the reduction in the level of the critical cleavage stress for the HAZ structures relative to the base plate, combined with the increase in the yield strength of the HAZ structure due to Nb addition.

Further Work

This project has demonstrated the potential to predict both Charpy and CTOD transition temperatures from a knowledge of the critical cleavage fracture stress and temperature dependence of yield stress. For the development of line pipe and offshore structural steels with improved HAZ toughness, it would be useful to accumulate data from both notch bend tests and instrumented impact tests on a variety of microalloyed chemistries, and HAZ microstructures and thermal treatments. These

data, combined with a knowledge of the corresponding temperature dependence of HAZ yield stress would enable a much more comprehensive view of the HAZ toughness to be developed.

Aside from microstructural-yield stress effects, a key consideration particularly for offshore steels, is the effect of section size (constraint) on fracture transition behavior. Little information is available in the effects of either thickness or ligament size. There is need to develop a test program (within the offshore industry) to characterize this effect as it relates to the fail safe design of large structures.

Finally, most of the work that Stelco-CANMET have done on the toughness of simulated HAZ structures has focused on the virgin or single thermal cycle. For multipass welding, particularly for offshore platform steels, the thermal history of most of the weldment is much more complex. It is clear that with microalloyed steels there is a strong potential for additional precipitation hardening in multipass welds and with stress relief treatments. In order to ensure that the measured values of the HAZ properties include the worst possible condition, this type of study should be extended to include determination of multipass effects.

ACKNOWLEDGMENTS

The authors wish to acknowledge the financial support of the Department of Supply and Services for funding this research. In addition they would like to thank Dr. J. T. McGrath and Dr. J. Bowker of PMRL, CANMET, for supplying the test steels and providing the Gleeble simulations and Dr. L. Collins of PMRL, CANMET for providing the dilatometer data. Special thanks are also due to the Stelco R&D machine shop, photographic lab, and B. Buck for preparing the test samples and this report.

REFERENCES

1. R. E. Dolby, G. G. Saunders: The Toughness of Weld HAZs, National Seminar, 1974, The Welding Institute, Cambridge, pp 43-66.

2. R. E. Dolby, M. W. F. Cane: ibid.

3. E. L. Banks: Toughness Properties of HAZ Structures in Structural Steel, Welding Research Supplement, July, 1974, p 299-S.

4. M. F. Gittos, R. E. Dolby: Welding Institute Members Report, 65/1978/M, May, 1978.

5. N. E. Hannerz: Effect of Nb on HAZ Ductility on Constructional HT Steels, Welding Journal Research Supplement, May, 1975, p 162-S.

6. N. E. Hannerz, B. M. Jonsson-Holmquist: Influence of Vanadium on HAZ Properties of Mild Steel, Metal Science, 1974, Vol 8, p 228.

7. R. E. Dolby: The Effect of Nb on HAZ Toughness of High Heat Input Welds in C-Mn Steels, The Welding Institute Research Bulletins, September, 1977, p 250.

8. S. Hasebe et al: The COD Value of Welding Joints in Line Pipe, Sumitomo Search, No. 12, November, 1974, pp 59-69.

9. A. B. Rothwell et al: Heat-Affected-Zone Toughness in High-Strength Pipeline Steels, 5th Bolton Landing Conference, Lake George, New York, August, 1978.

10. P. Bufalini, F. Bonomo, C. Parrini: Effects of Composition and Microstructure on HAZ Toughness and Cold Cracking, BTF-Maggio 1977, p 337.

11. H. Gondoh et al: Recent Progress in Acicular-Ferrite Steels for Arctic Grade Line Pipe, 16th CIM Conference, Vancouver, 1977.

12. MIG SAW Process for Pipe Seam Welding, Sumitomo Metal Industries, December, 1978.

13. N. Takahashi et al: Developments of Seam Welding of High Test Line Pipe, Nippon Kokan KK, 1976.

14. D. B. McCutcheon et al: "Improvement of SAW HAZ Toughness by Ti Additions to Line Pipe Steels," paper presented at Micon 82, Houston, Texas, January, 1982.

15. D. B. McCutcheon et al: "The Effect of Microalloy Additons on the HAZ Notch Toughness of a C-Mn-Mo Line Pipe Steel", presented at 1983 International Conference on Technology and Applications of HSLA Steels, Philadelphia, Pa, Oct, 1983.

16. L. G. Luo et al: "On the Development of a Direct Method of Determining the Microcrack Resistance Curve", paper accepted by Engineering Fracture Mechanics.

17. E. Orowan: "Trans Inst Engrs, Shipbuilders Scot.", 89, 165, (1945).

18. A. H. Cottrell: "Trans Am Inst Min Metall Petrol Eng, 212, 1982, 1958.

19. L. M. Brown and H. R. K. Ham: Strengthening Mechanisms in Crystals, edited by A. Kelly and R. B. Nicholson, published by Elsevier Press, 1971, p 30.

20. E. A. Almond, J. T. King, J. D. Embury: Metallography, 1970, Vol 3, p 1.

21. J. Malkin and A. S. Tetelman: "Eng Fracture Mechanics, 3, 1971, 2, pp 151-167.

22. E. A. Almond et al: "Fracture 1969", Proc Second Int Conference on Fracture, 253, Chapman and Hall, London, (1969).

23. S. T. Rolfe and J. M. Barsom: "Fracture and Fatigue Control in Structures", Prentice Hall, 1977, p 103.

Table I: Chemical Compositions (%)

Steel	C	Mn	S	Si	Mo	Nb	Ti	N	ASA
449	0.066	1.82	0.005	0.24	0.33	-	0.010	0.008	0.018
460	0.078	1.76	0.005	0.24	0.33	0.015	0.011	0.007	0.013
454	0.075	1.86	0.005	0.24	0.33	0.044	0.010	0.007	0.010

Table II: HAZ Transformation Data ($\Delta T_{800-500}$ = 22 sec)

Steel	% Nb	Temperature at % Transformation (°C)		
		Start	50%	Finish
449	0	615	565	440
460	0.015	610	550	420
454	0.044	590	540	395

Table III: HAZ CTOD Transition Data - Minimum CTOD (mm) at Test Temperature (°C)

Steel	% Nb	52	22	-4	-17	-32
449	0	NA	0.22	0.14	0.06	0.06
460	0.015	0.26	0.17	0.09	0.07	0.05
454	0.044	0.21	0.11	0.05	0.06	0.05

Table IV: Prediction of Base Plate and HAZ 20 J Transition Temperature

Condition	Steel	% Nb	Room Temperature σ_{YS} (MPa)	Predicted 20 J TT (°C)	Actual 20 J TT (°C)
Base Plate	449	0	350	-149	-150*
	460	0.015	400	-140	"
	454	0.044	450	-131	"
HAZ	449	0	550	-31	-40
	460	0.015	575	-15	-10
	454	0.044	600	2	0

* estimated from extrapolation of Charpy data from -100°C.

Table V: HAZ CTOD Crack Initiation Mechanism Transition Temperatures

Steel	% Nb	δ_i (mm)	δ_{cleav} (mm)	T_i (°C)
449	0	0.20	∞	<24
460	0.015	0.20	0.3	≈24
454	0.044	≈0.20	0.1 - 0.17	>24

Table VI: HAZ CTOD Transition Temperatures

Steel	Nb Level	σ YS (MPa)	Predicted	Actual*
			T_i (°C)	T_i (°C)
449	0	550	10	5
460	0.015	575	25	25
454	0.044	600	70	40

* Estimated from minimum value CTOD transition curves.

Figure 1: Orientation of the tensile, Charpy and CTOD specimens

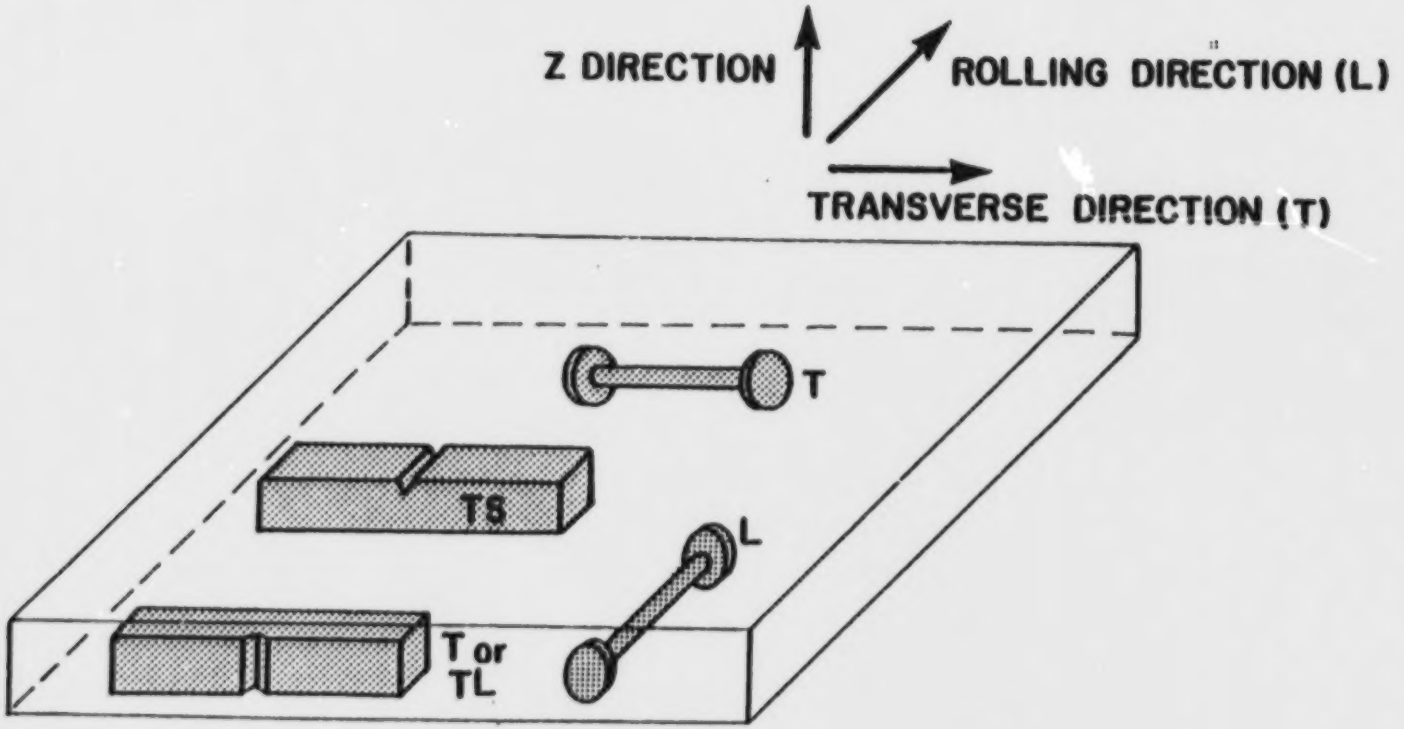

Figure 2: Pre-cracked CTOD specimen in the three point bend rig

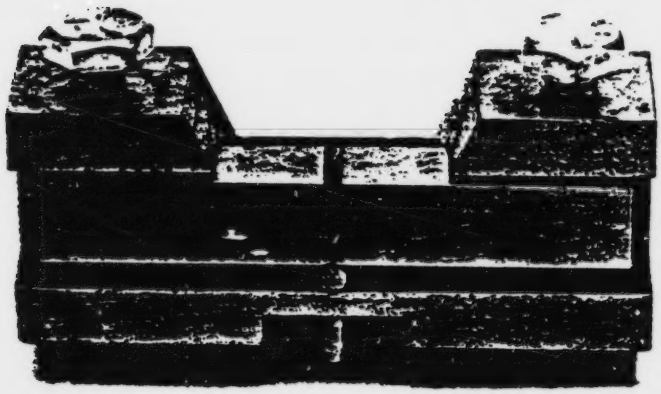

Figure 3: Void growth along the fatigue crack tip during incremental loading

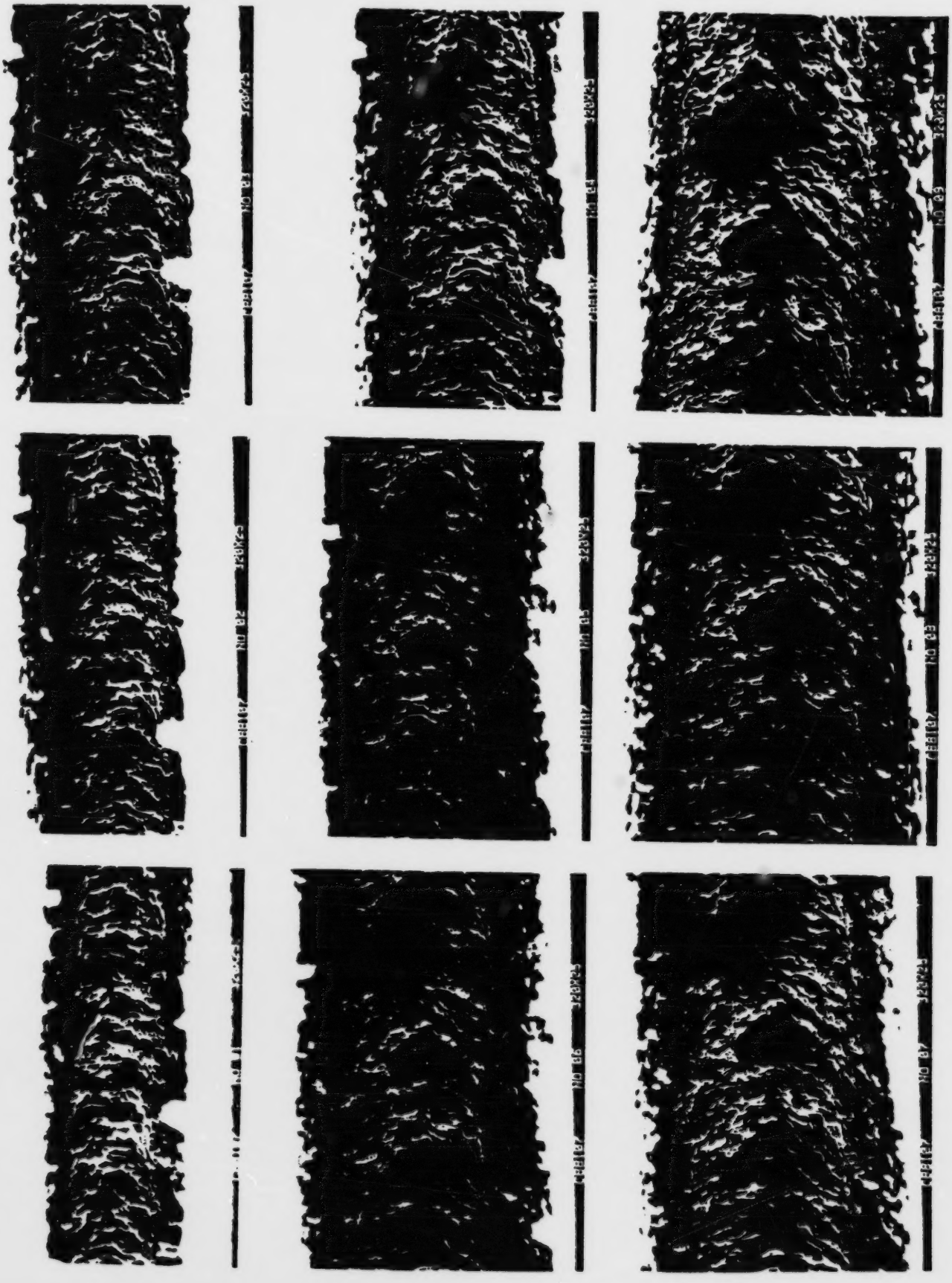

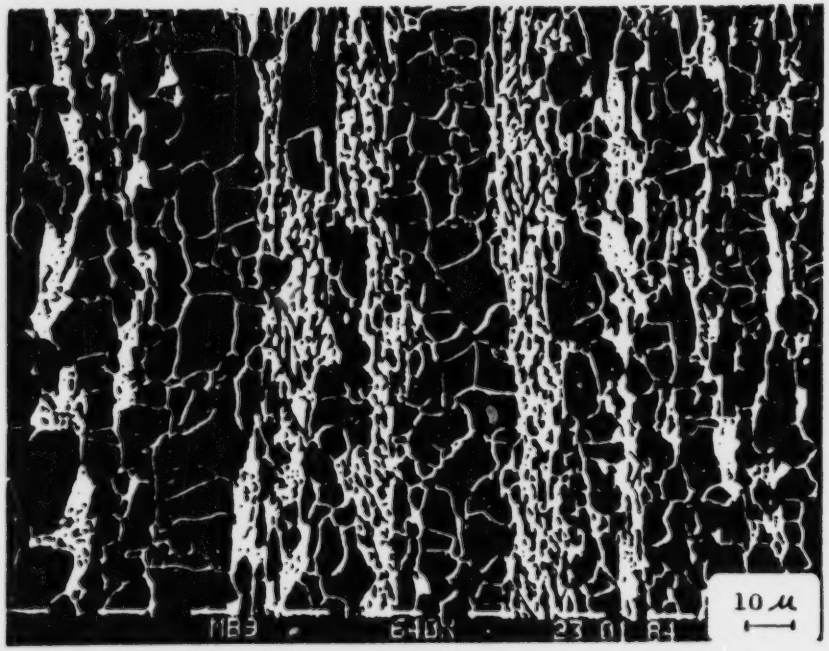

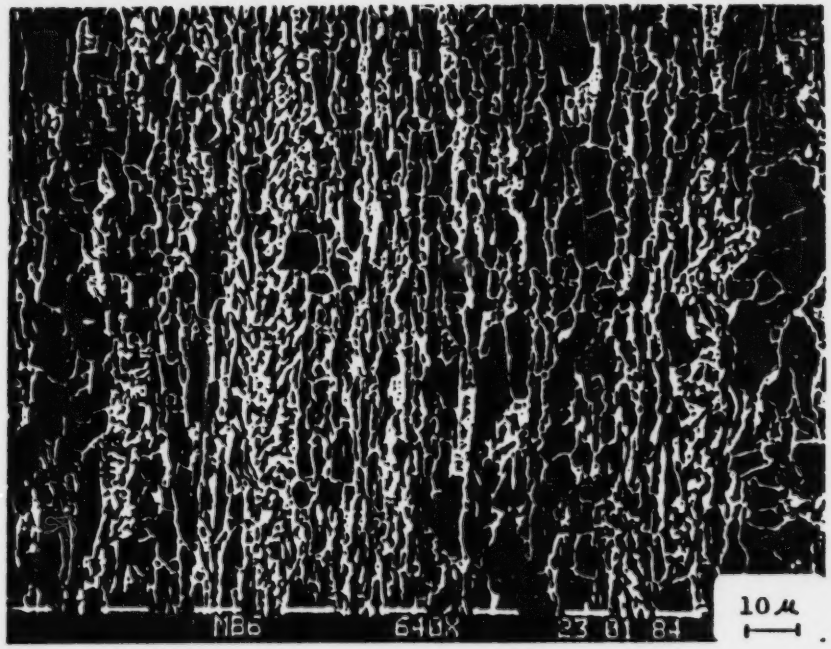

Figure 4(a): SEM Micrographs Showing the As-Rolled Plate Microstructures of:

(a) Steel 449, 0 Nb
(b) Steel 460, 0.015 Nb
(c) Steel 454, 0.044 N

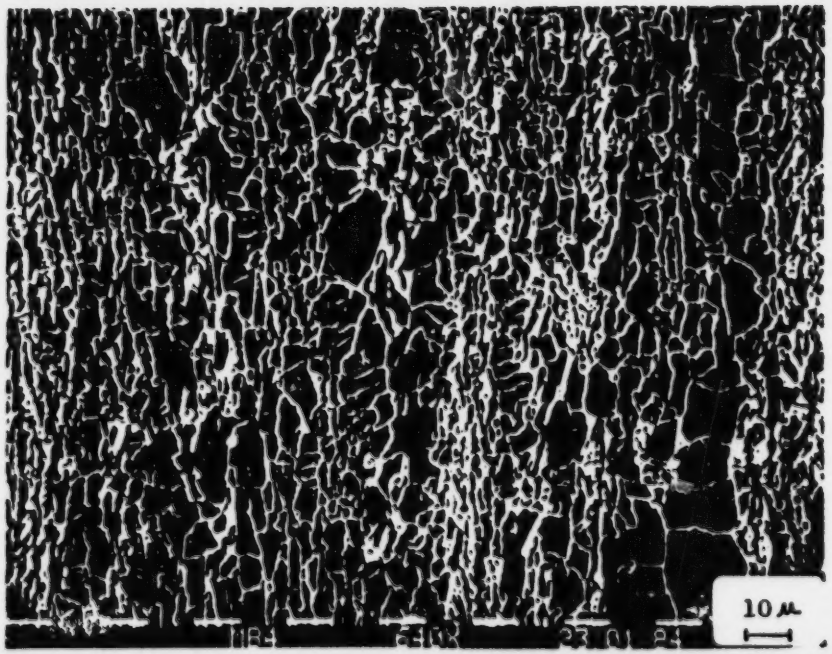

Figure 4b: TEM micrographs of the as-rolled plates

(a) Steel 449, 0 Nb; (b) Steel 454, 0.044 Nb

Figure 5: Microstructures of Gleeble simulated HAZ

(a) Steel 449, 0 Nb (X500)

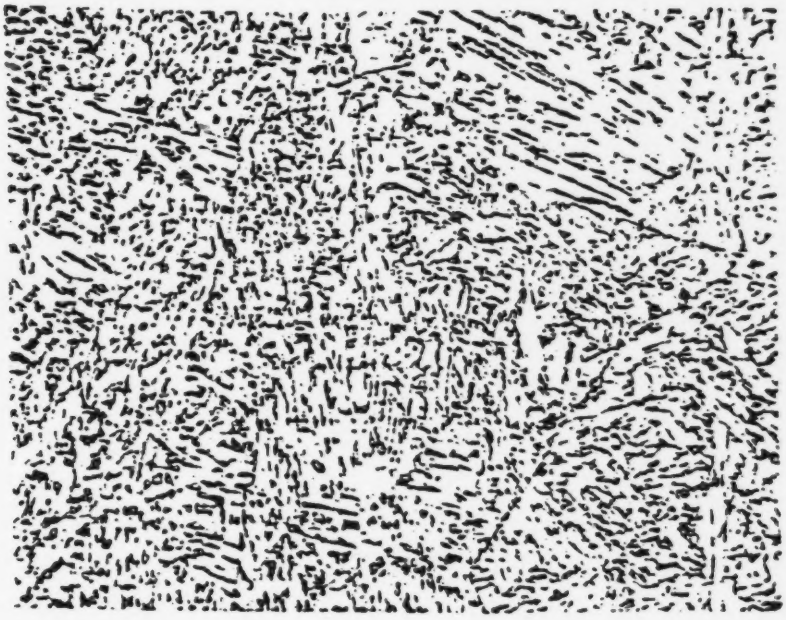

(b) Steel 454, 0.044 Nb (X500)

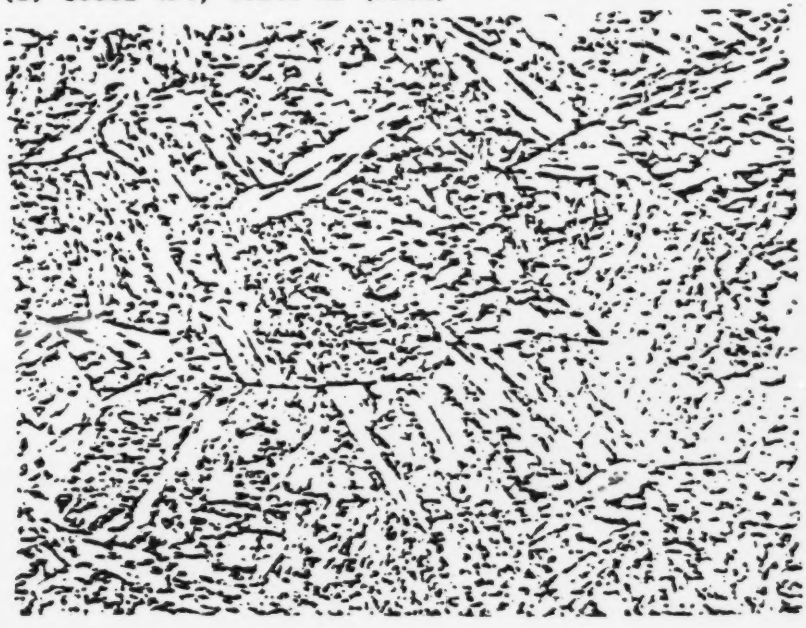

Figure 6: Histograms of prior austenite grain size of the Gleeble simulated HAZ samples

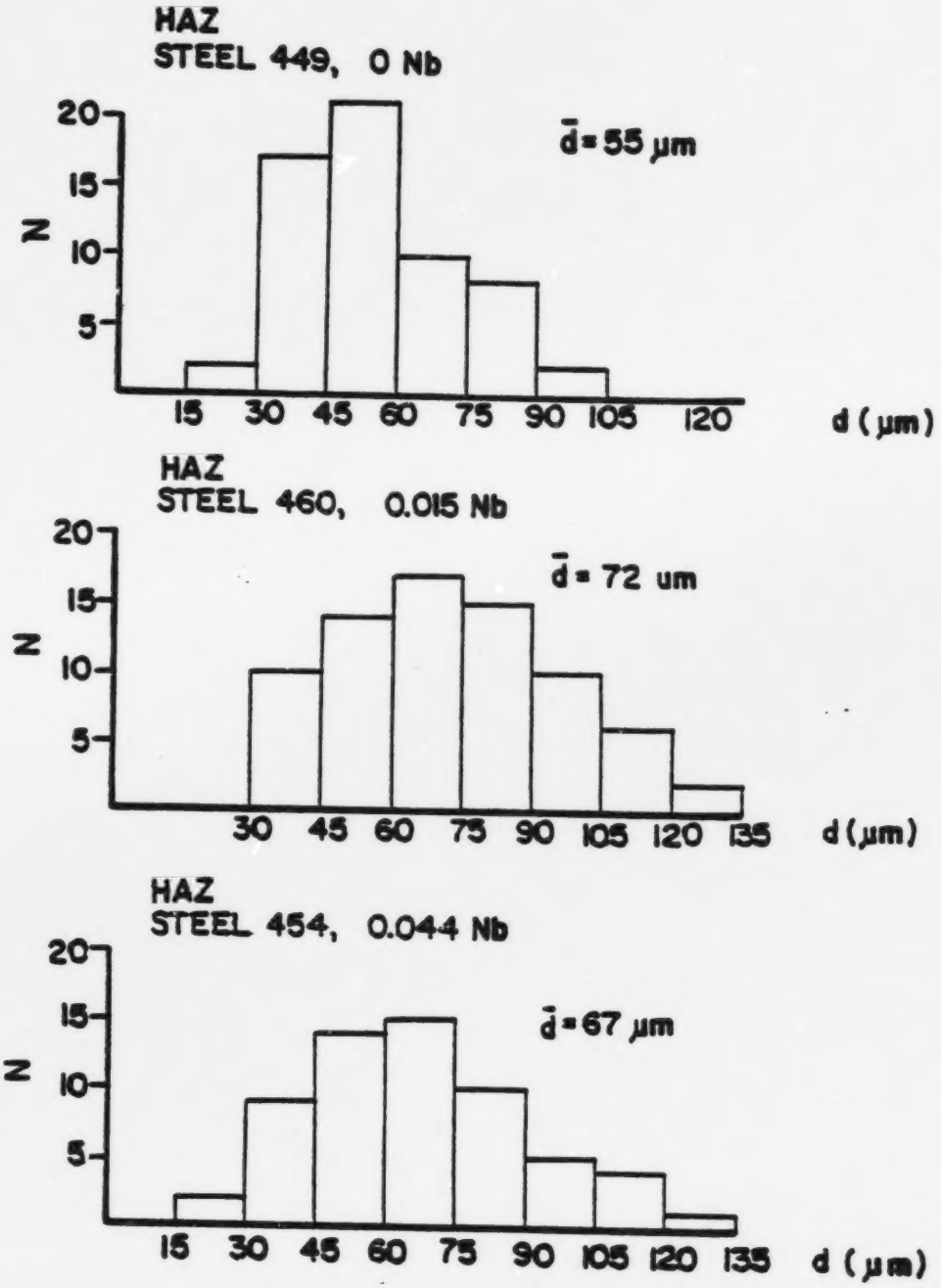

Figure 7a: The yield and ultimate stresses (a-1), and fracture strains (a-2) versus temperature for longitudinal specimens

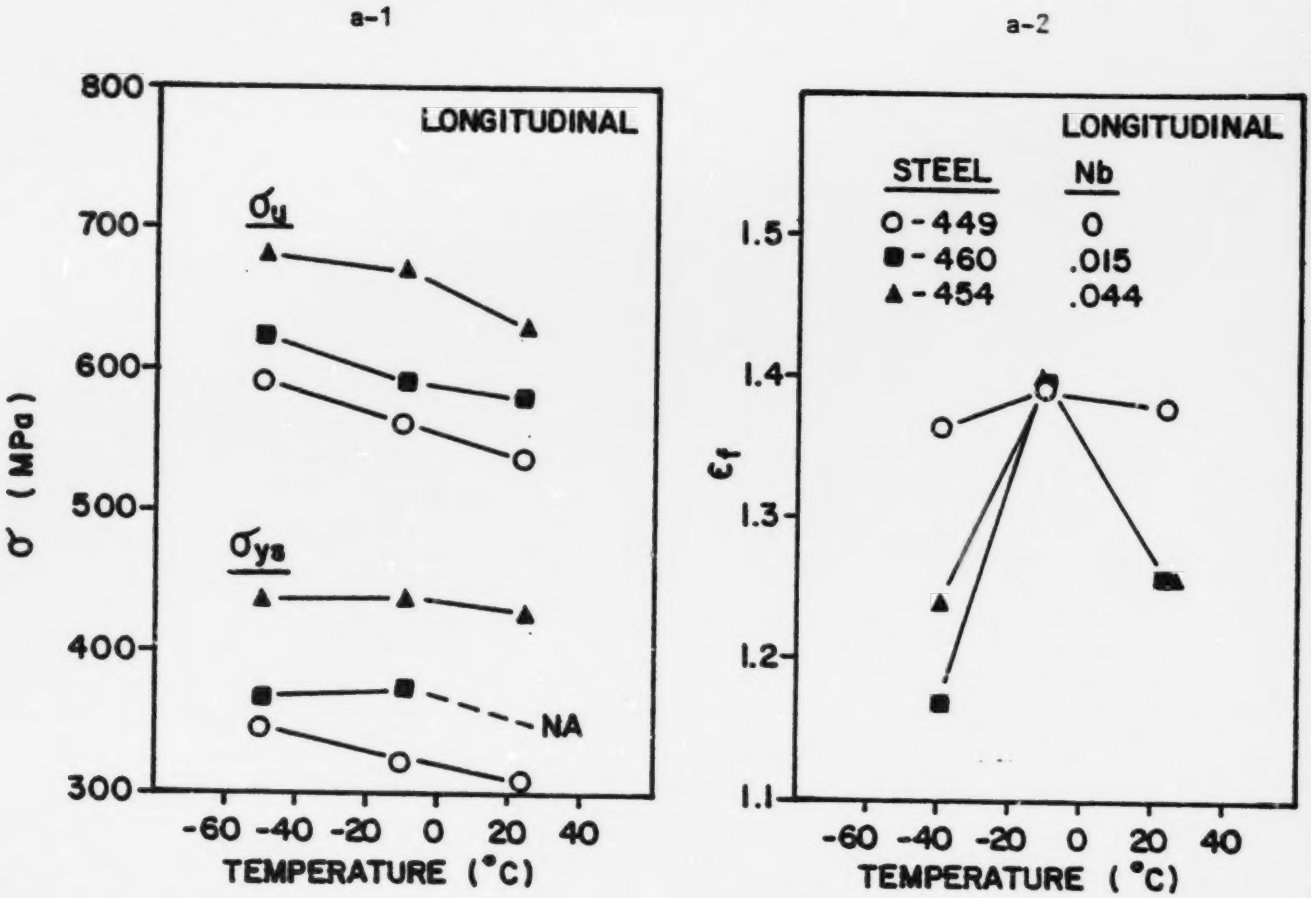

Figure 7b: The yield and ultimate stresses (b-1), and fracture strains (b-2) versus temperature for transverse specimens

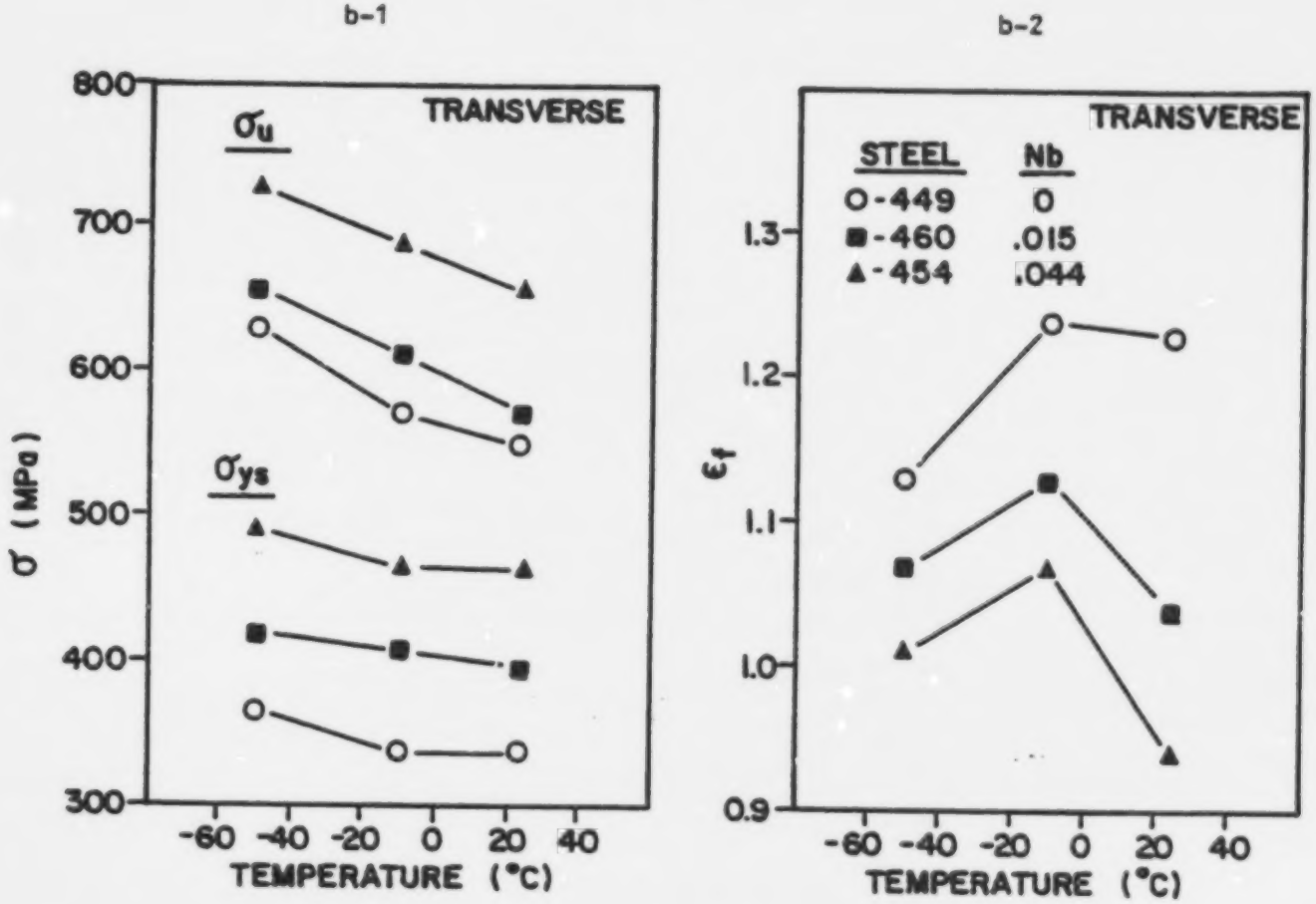

Figure 8: The yield and ultimate stresses (a), and fracture strains (b) versus temperature for simulated HAZ structure

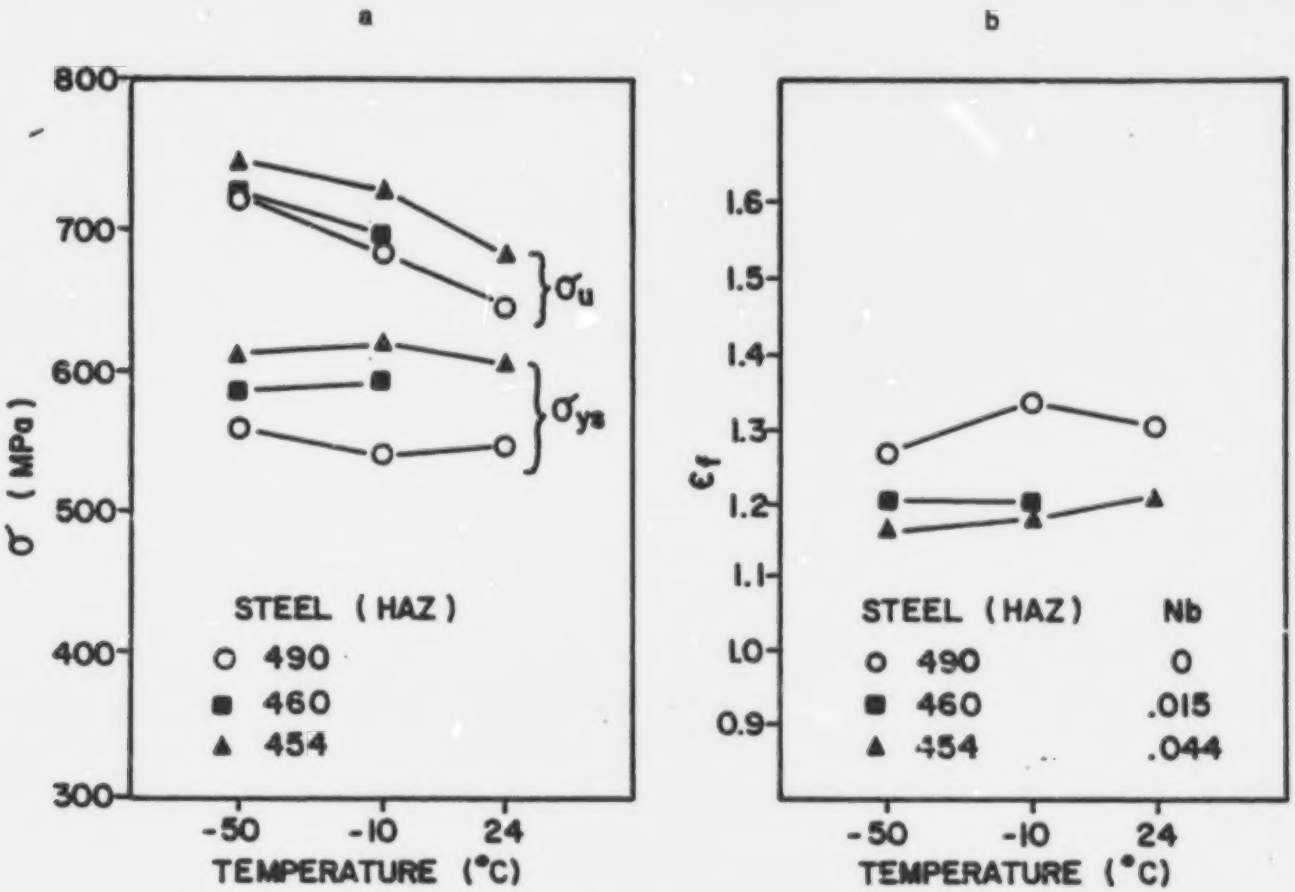

Figure 9: Charpy impact transition curves in the as-rolled condition

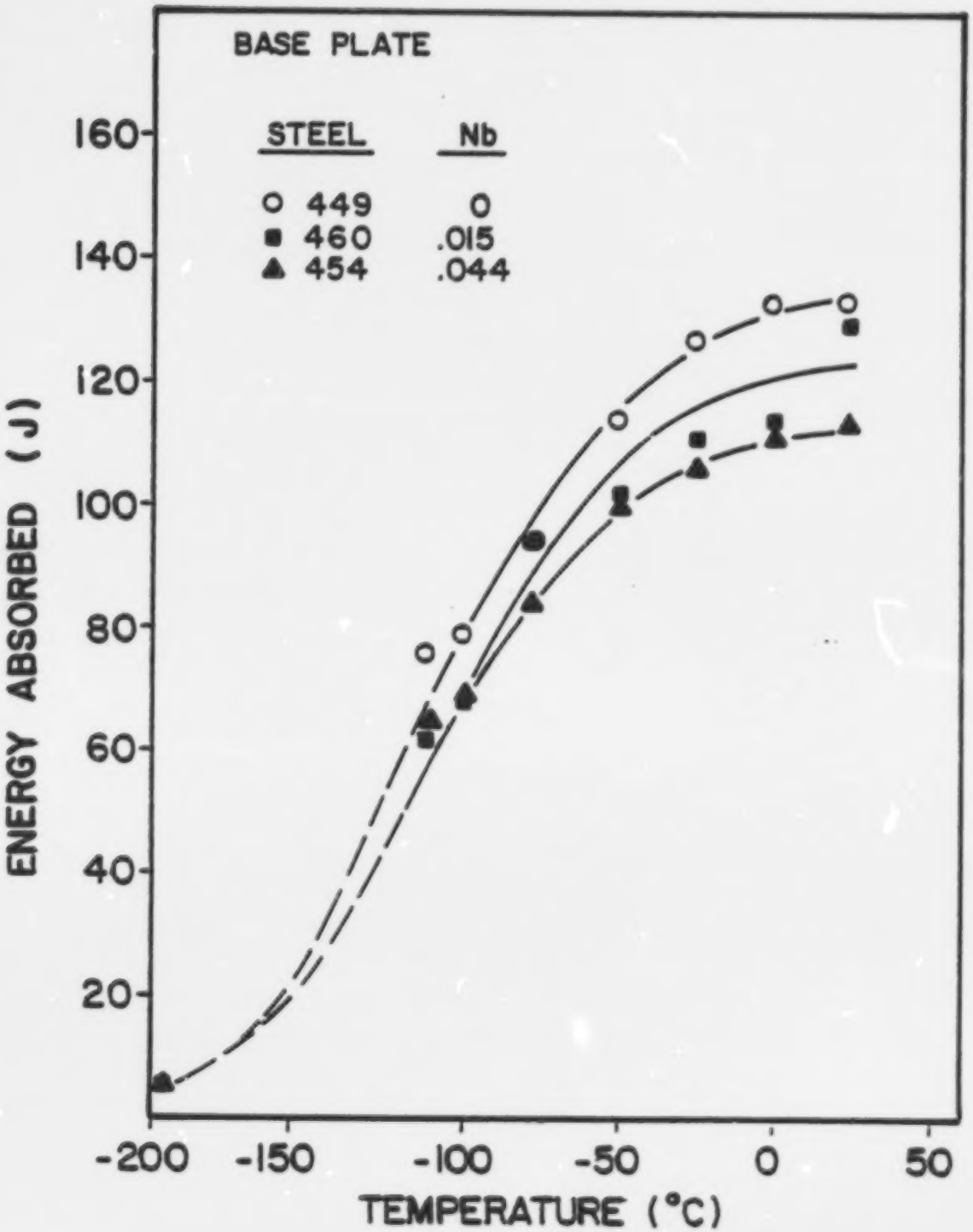

Figure 10: Charpy impact transition curves of the simulated HAZ structures

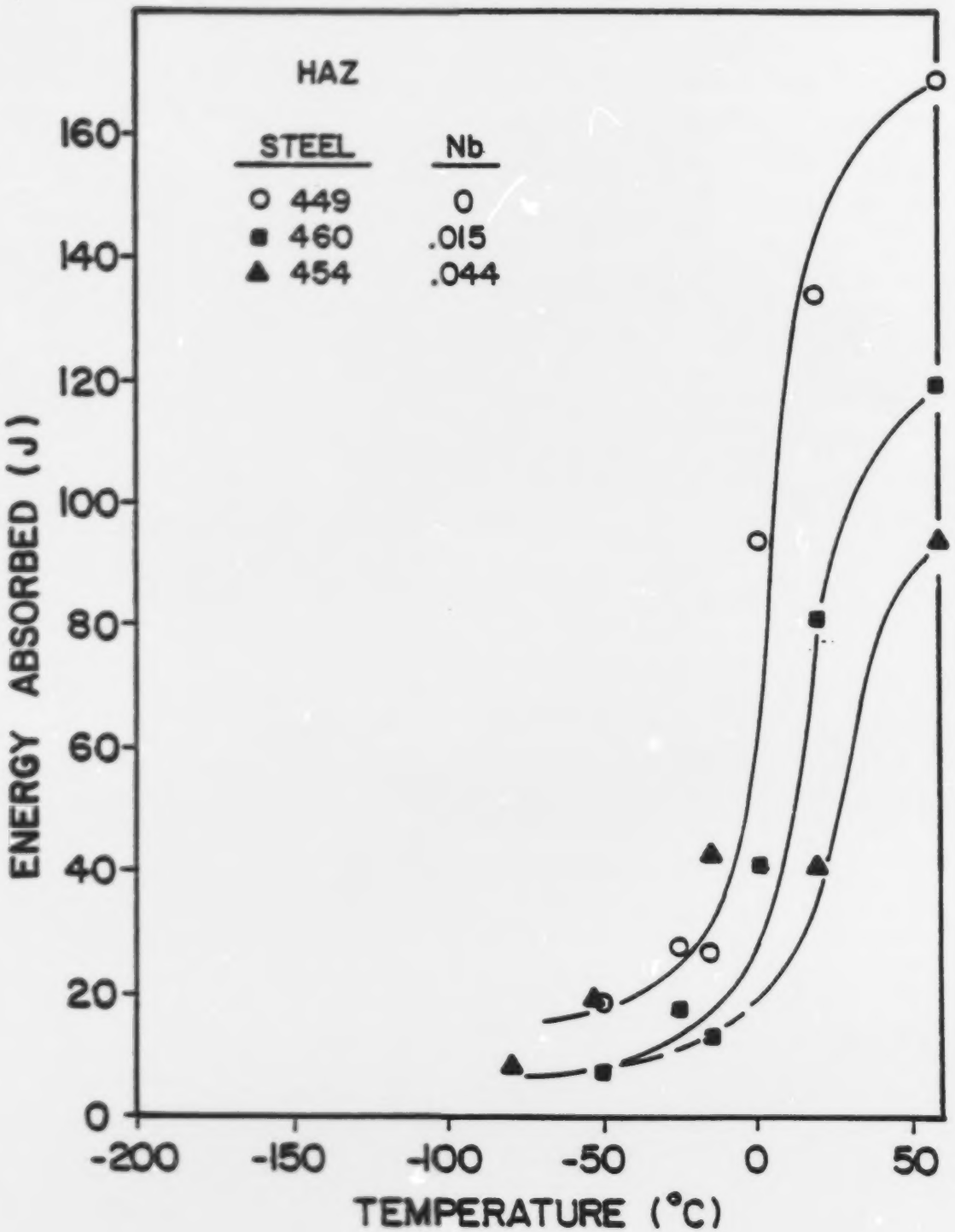

Figure 11a: Cleavage facets on the fracture surface of a Charpy specimen of base plate 449 fractured at -196°C

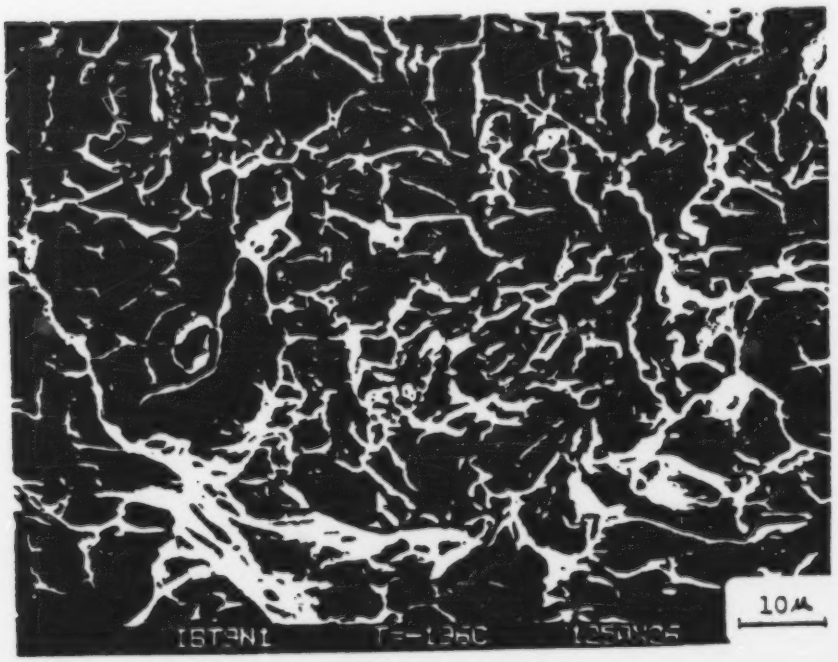

Figure 11b: Cleavage facets of the fracture surface of a HAZ Charpy specimen fractured at -50°C (steel 449)

Figure 12: SEM micrograph showing the cleavage fracture surface and microstructure for an HAZ CTOD specimen (steel 454)

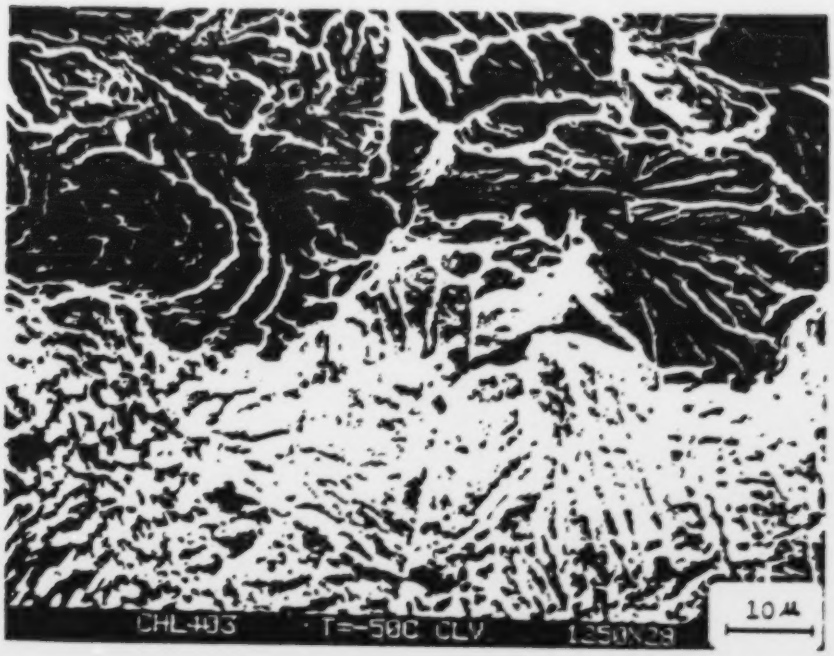

Fracture Surface

Etched Microstructure

Figure 13: Histograms of the cleavage facet size for the as-rolled plates

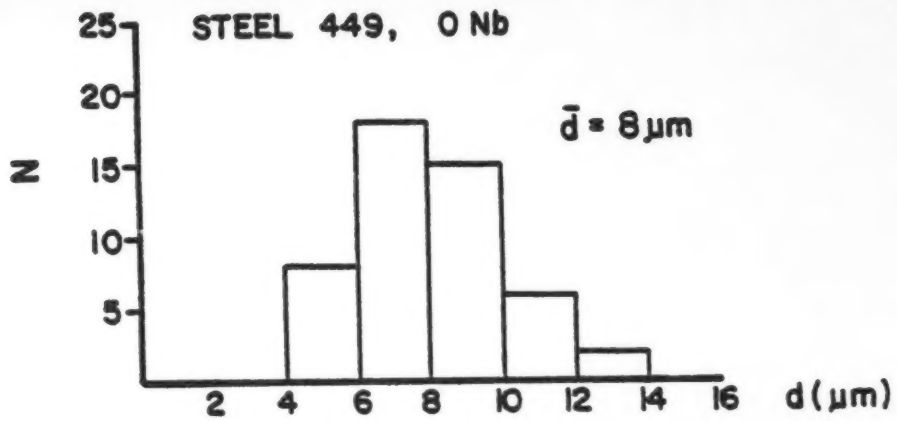

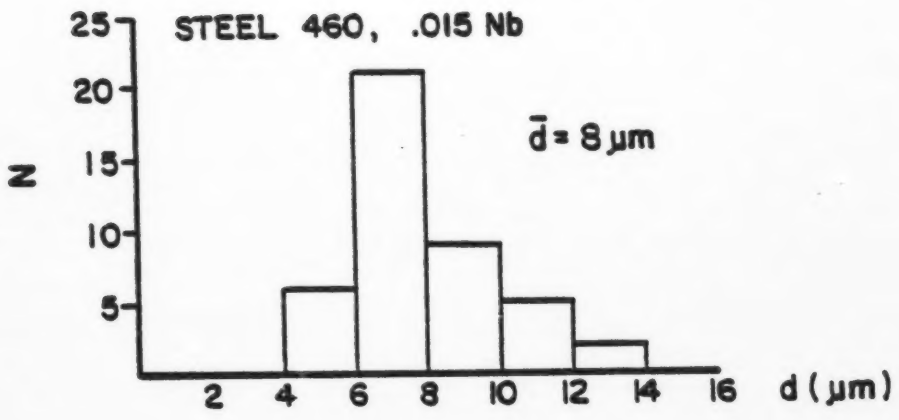

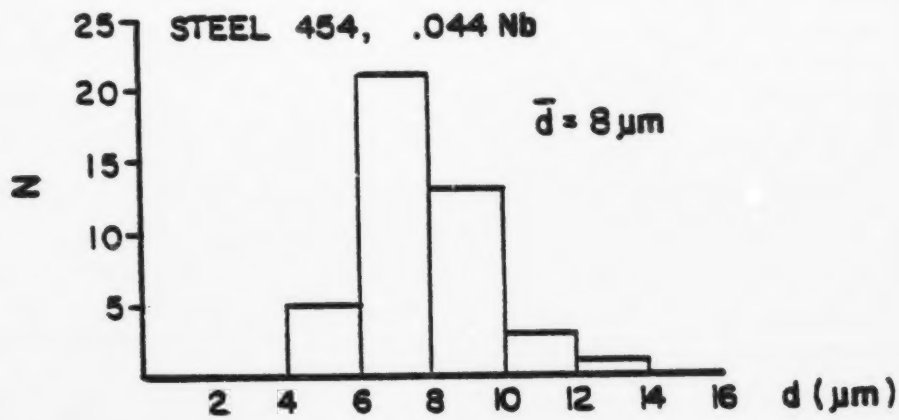

Figure 14: Histograms of the cleavage facet size for Gleeble simulated HAZs

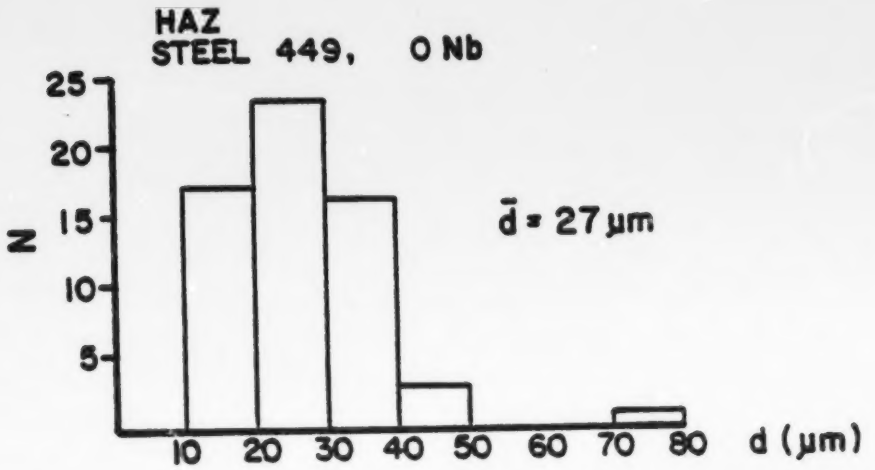

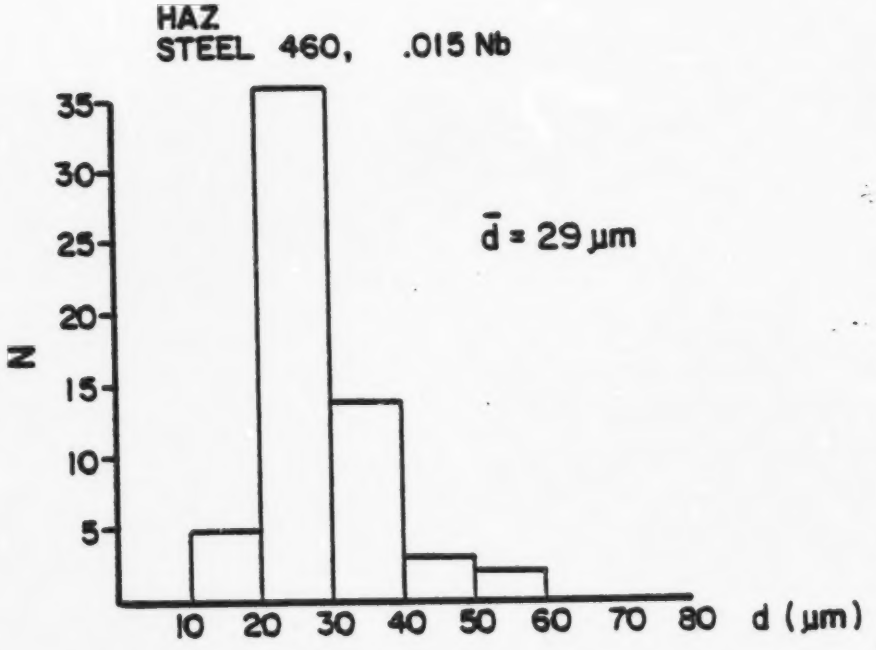

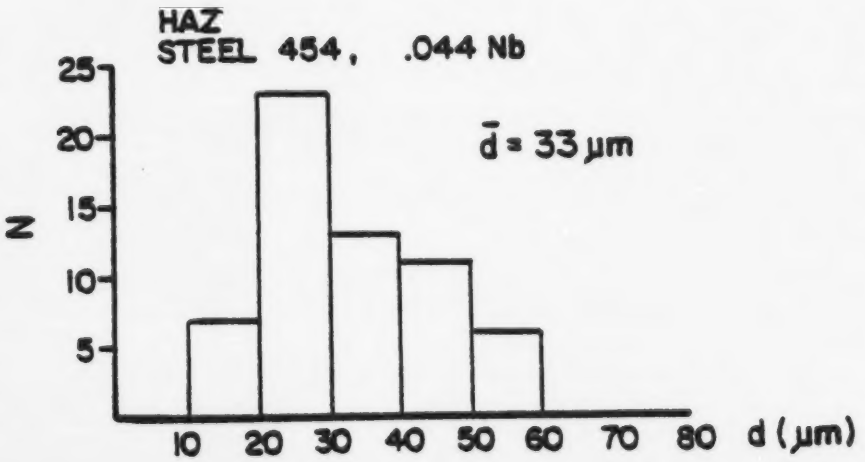

Figure 15: Fracture surfaces of Charpy impact specimens tested at various temperatures for as-rolled plates of (a) steel 449, (b) steel 460 and (c) steel 454

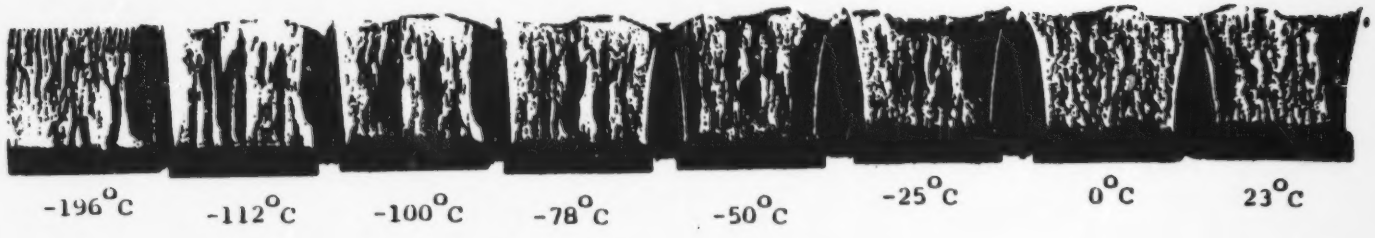

(a)

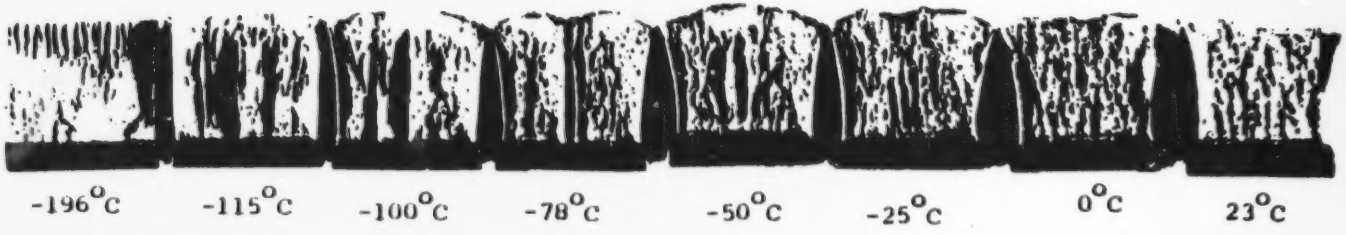

(b)

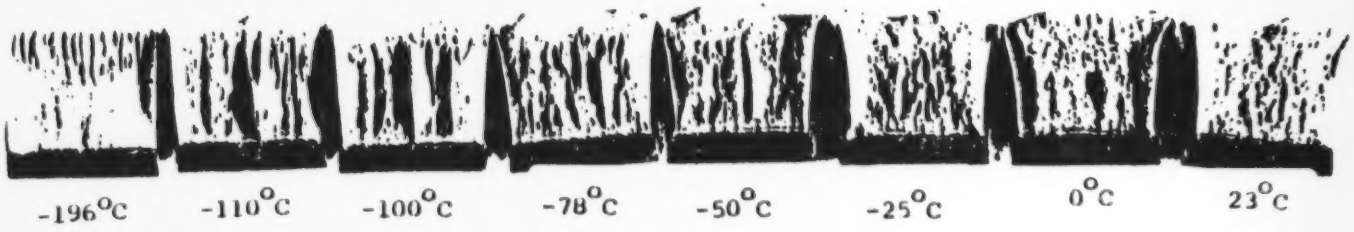

(c)

Figure 16: Fracture surfaces of Charpy impact specimens tested at various temperatures for Gleeble simulated HAZs of (a) steel 449, (b) steel 460 and (c) steel 454

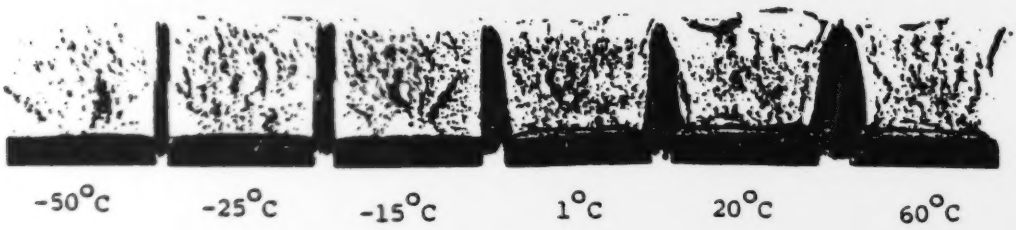

(a)

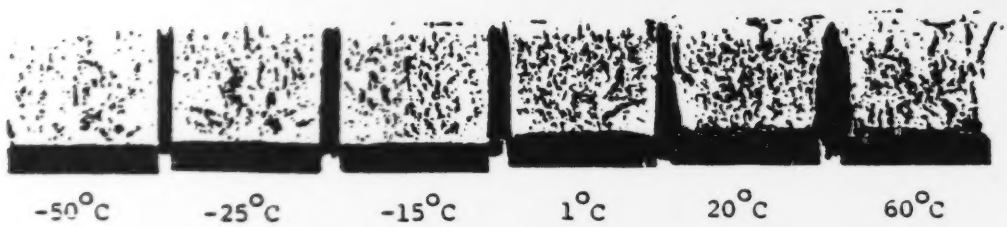

(b)

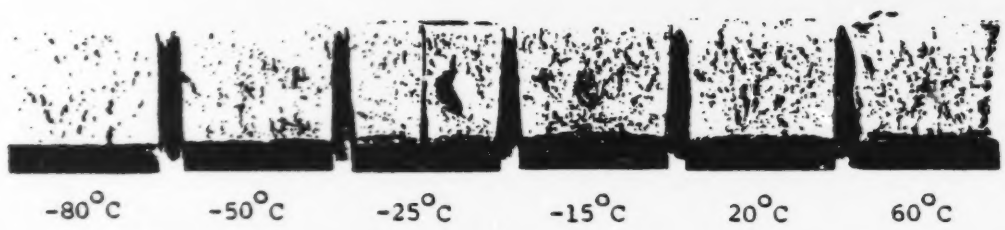

(c)

Figure 17: Micro- and macro-crack CTOD resistance curves of as-rolled plates (TL direction, room temperature tests)

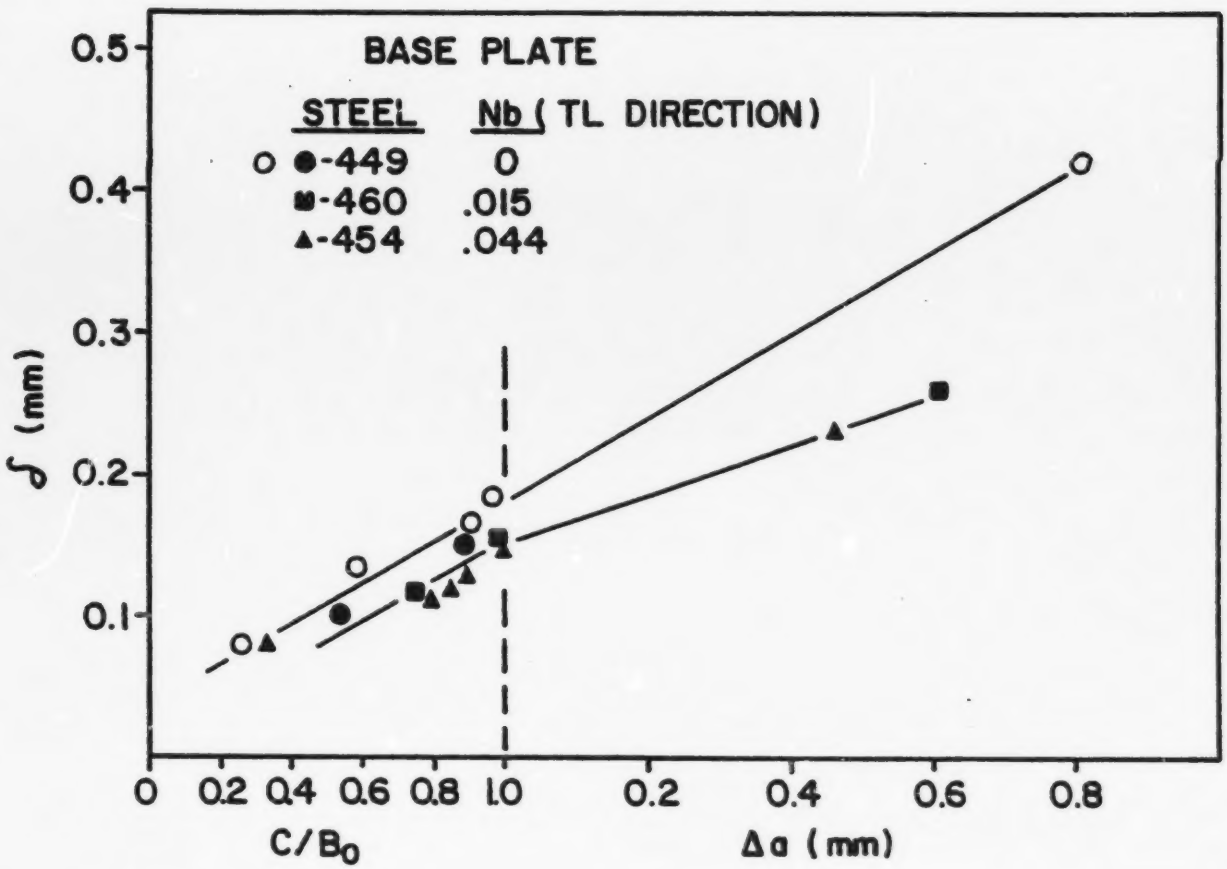

Figure 18: Micro- and macro-crack CTOD resistance curves of as-rolled plates (TS direction, room temperature tests)

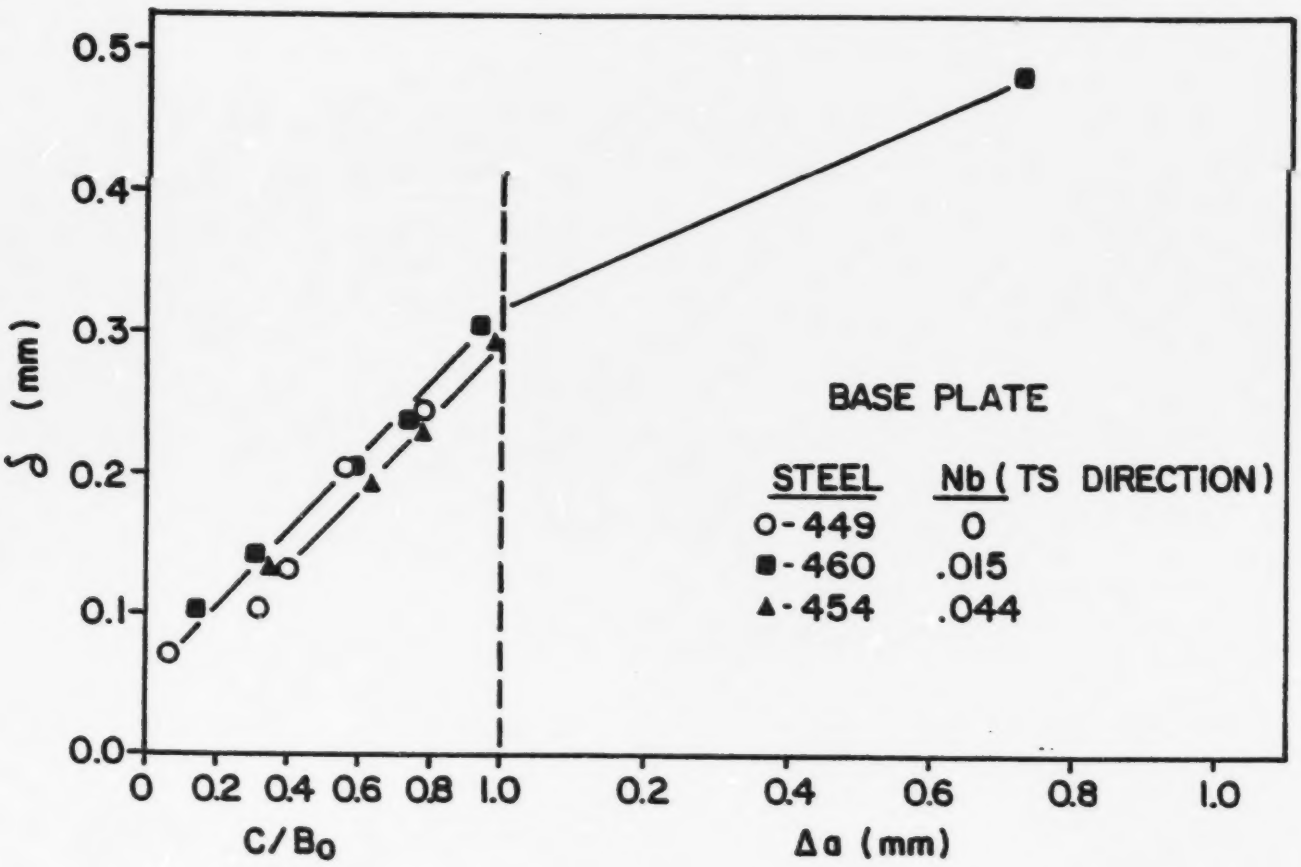

Figure 19: Micro- and macro-crack CTOD resistance curves of simulated HAZ structures (TL direction, room temperature tests)

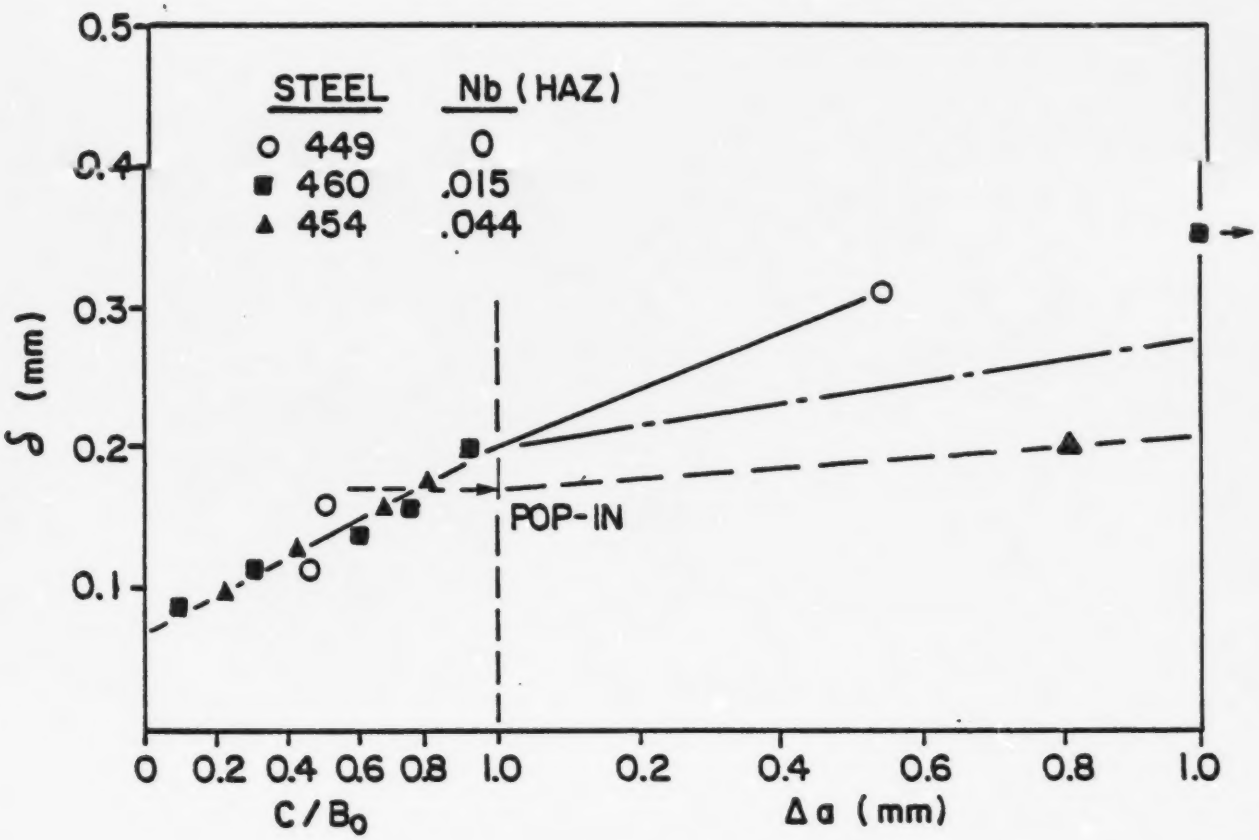

Figure 20: Voids nucleated at inclusions in a Gleeble simulated HAZ sample (steel 454)

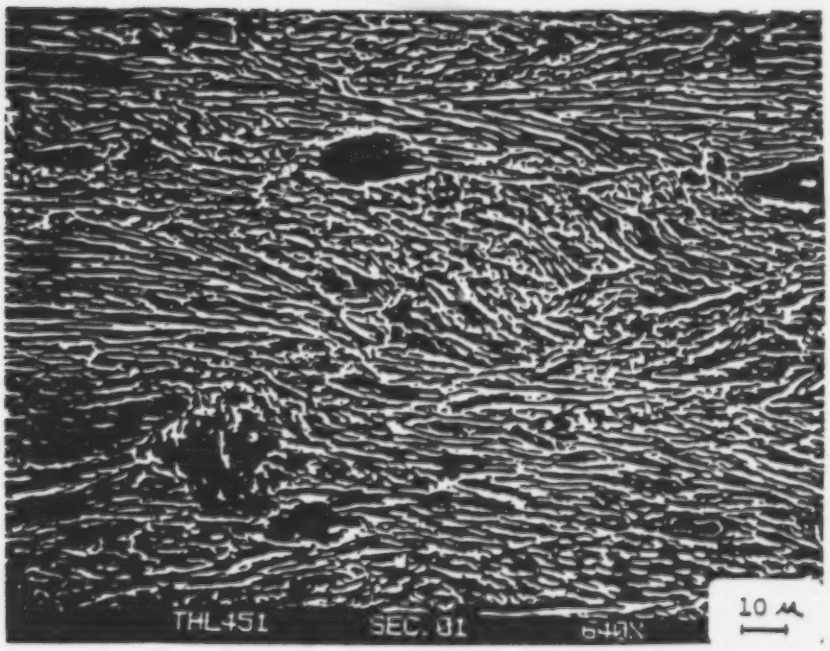

Figure 21: Theoretical prediction of the cleavage stress as a function of grain size and carbide thickness

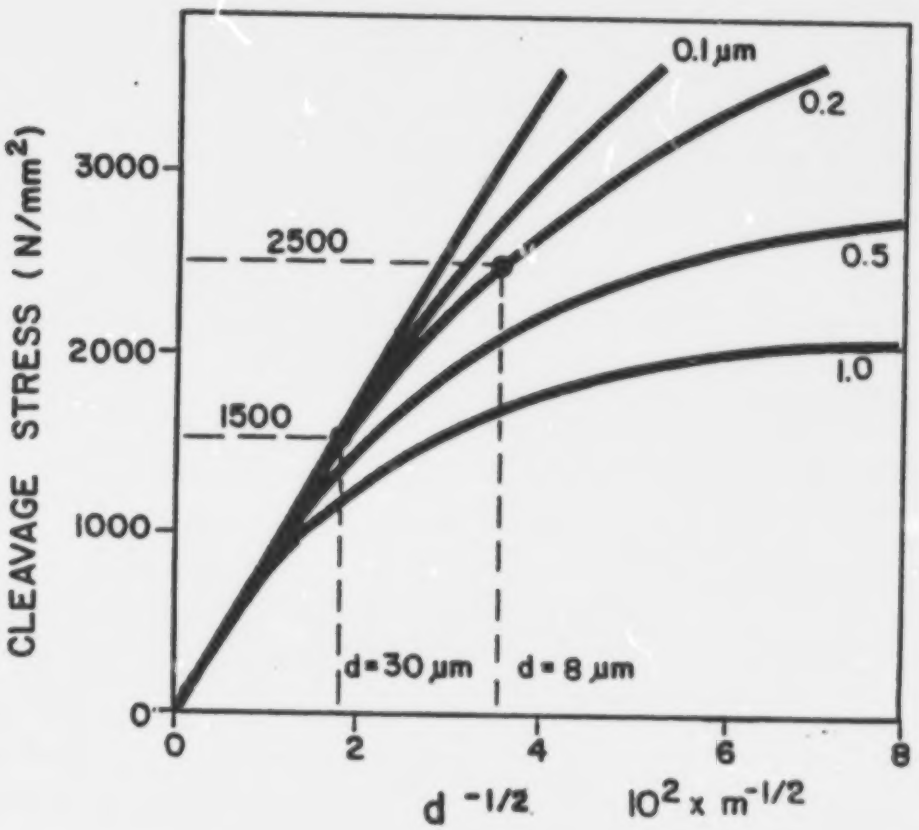

Figure 22: Schematic diagram showing the difference in transition temperatures between as-rolled plates and simulated HAZ structures

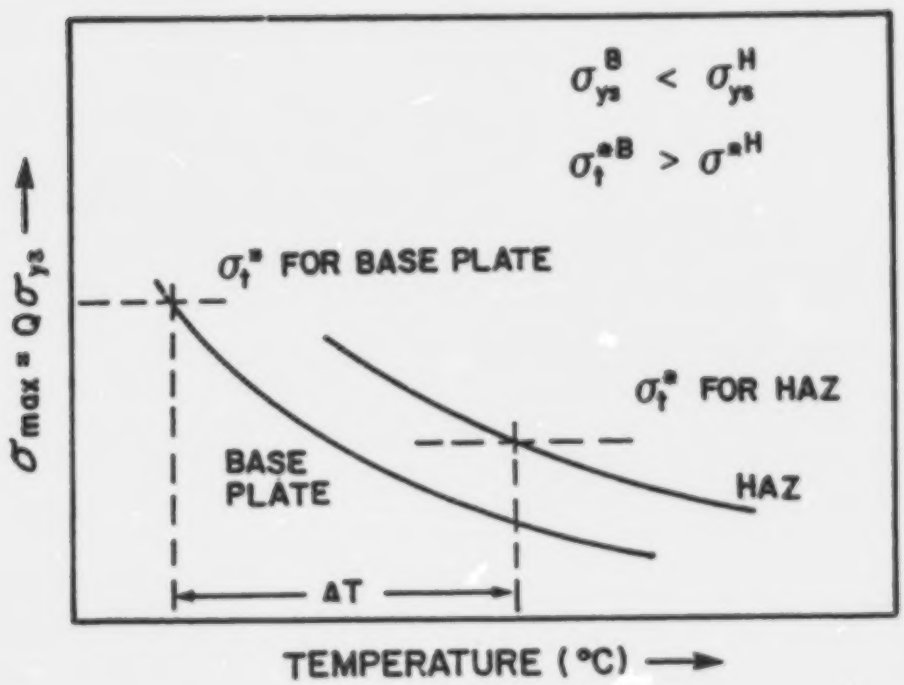

Figure 23: Predictions of transition temperatures of as-rolled plates and simulated HAZ structures

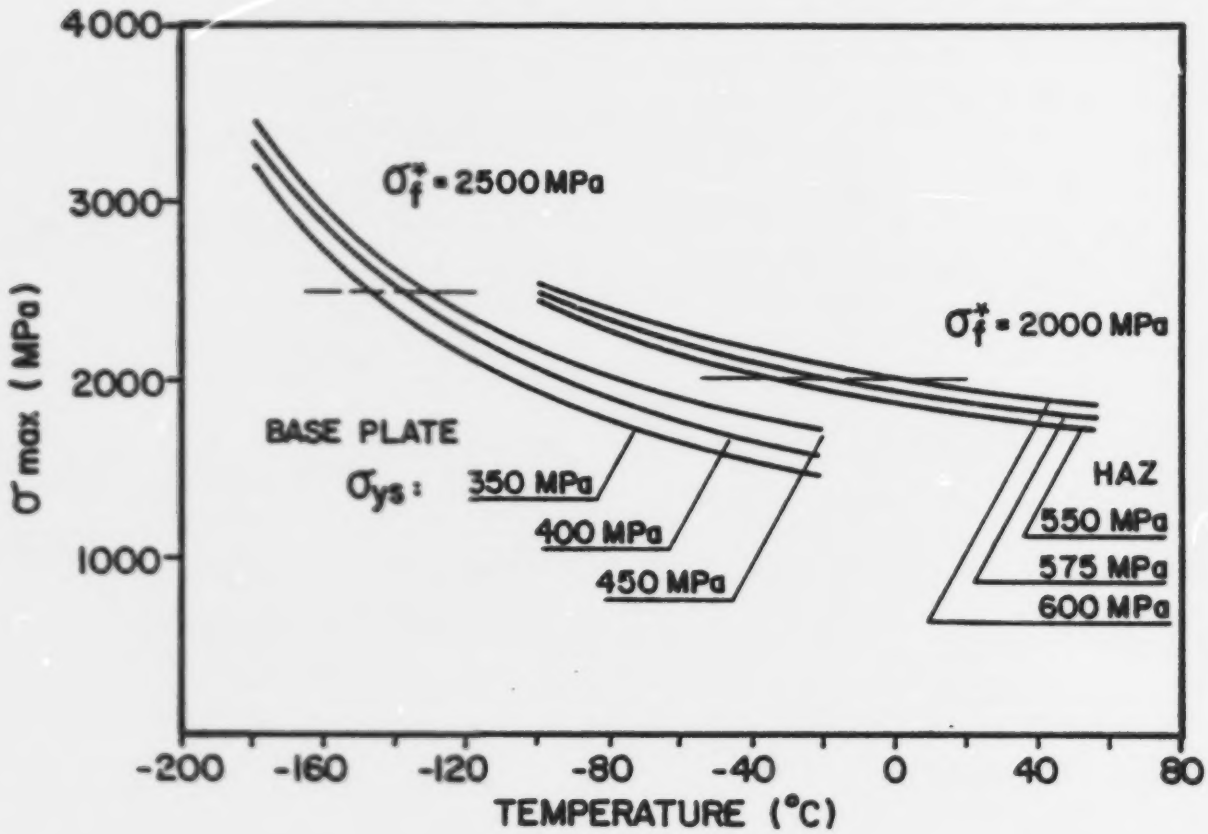

Figure 24: Schematic diagram showing the CTOD transition curve and the corresponding fracture mechanism transition temperatures

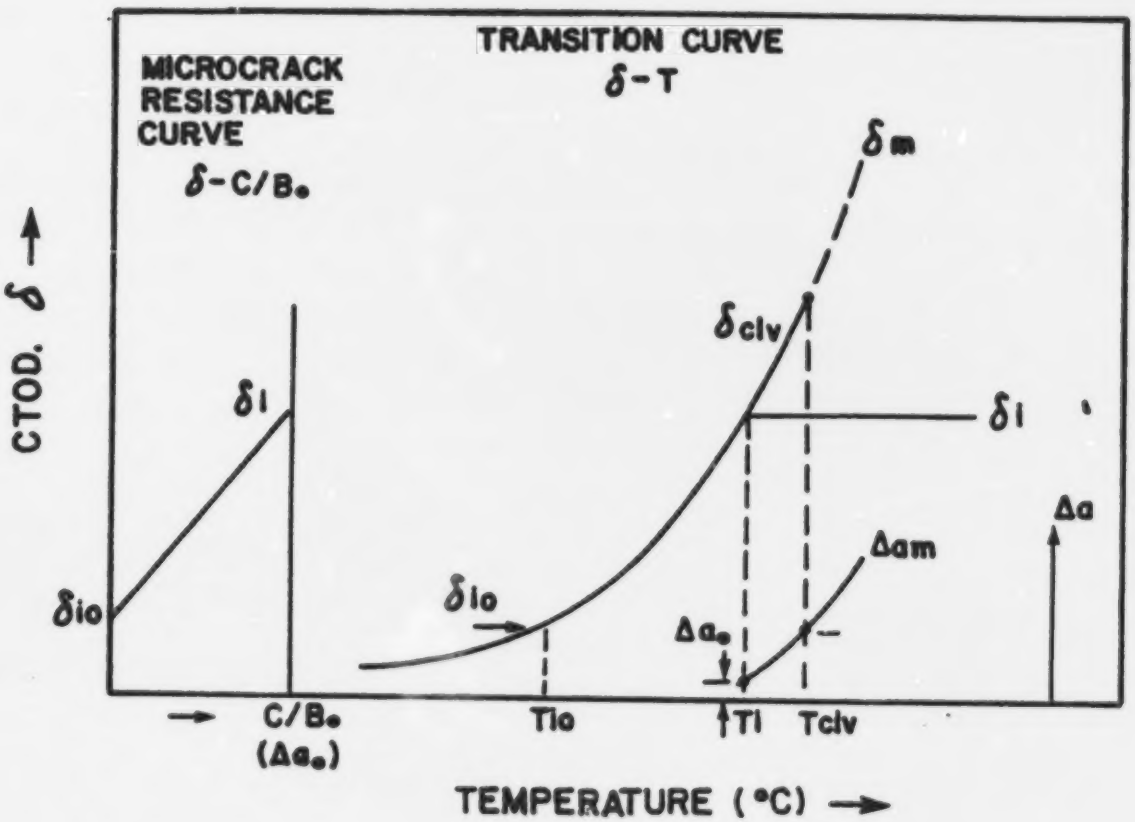

Figure 25: Schematic diagram showing the fracture modes of the simulated HAZ structures tested at room temperature